CREATING A BOSE-EINSTEIN CONDENSATE OF STABLE MOLECULES USING PHOTOASSOCIATION AND FESHBACH RESONANCE

A Dissertation
Submitted to
the Temple University Graduate Board

In Partial Fulfillment
of the Requirements for the Degree of
Doctor of Philosophy

---

by
Pierre Phou
May, 2014

Examining Committee Members:

Andreas Metz, Advisory Chair, Department of Physics
Theodore Burkhardt, Department of Physics
Dmitri Romanov, Department of Physics
Matt Mackie, External Examiner

ABSTRACT

Quantum degenerate molecular gases are of interest for the unique level of control they offer over chemical interactions and processes. To reach the quantum degenerate regime, these molecular gases must be cooled to ultracold temperatures, typically on the order of 100 nanoKelvins. Unlike atoms, with a few-level system that facilitates cooling, molecules represent a many-level system, which makes these temperatures experimentally difficult to achieve. As a result, experiments have turned to photoassociation and Feshbach resonance as shortcuts to form ultracold molecules from already ultracold atoms. Photoassociation and Feshbach resonance have been utilized to successfully create stable quantum degenerate molecules, but not on a routine basis, and only for a small range of molecular species. The primary focus of this thesis will be to study photoassociation and Feshbach resonance, and investigate possible routes to more efficient long-lived quantum degenerate molecule formation. We will also investigate realistic limiting conditions to open the possibility to more routine molecules, and to molecular species that are currently inaccessible. Overall, we find combined photoassociation and Feshbach resonance are viable schemes for efficiently creating quantum degenerate molecules, under realistic restrictions such as low laser intensity, narrow Feshbach resonance, and strong elastic collisions. As the techniques to create quantum degenerate molecules become more robust and experimentally available, the creation of colder, larger, and more long-lived samples will facilitate study of these molecules, and spur development into new applications.

DEDICATION

To my wife, Racine, and son, Aleem

who make every day special.

ACKNOWLEDGEMENTS

To all my family and friends, I am forever grateful for all the encouragement and support over the years. First and foremost, to my wife, Racine, who has given me more love and support in this endeavor than I can ever hope to return. To my son, Aleem, who makes all the hard work worthwhile, and displays a curiosity for life, even at such a young age, that reminds me why I pursued physics in the first place. And, to my parents, who have always put my education ahead of their own wants and needs.

I also want to thank my primary advisor, Matt Mackie, whose constant guidance has allowed me to grow and develop as a physicist in ways I never could have imagined. His tutelage was of such high caliber that, at times, I felt I was learning lessons not just in physics, but in life as well. At times I even felt like I was playing Foreman to his House. On the other hand, when I found myself stuck and feeling discouraged, he always had words of encouragement that kept me going and restored my resolve. Without his support, I do not think I ever would have made it this far.

I must also express my thanks to my current advisor, Andreas Metz, whose generous support goes above and beyond anything I could have hoped for. His counsel and frequent advising sessions have kept me motivated and producing more than I would likely have produced on my own. His questions and observations have also been extremely insightful in providing perspective and helping me identify the areas where I need to focus and know how to come up with answers. I am incredibly fortunate to have had him as a teacher and advisor.

Finally, I want to thank the whole Physics Department faculty. So many of you have offered me assistance or expressed your support throughout the years, which has been a tremendous boost for my confidence. To all of you and more, thank you.

TABLE OF CONTENTS

LIST OF TABLES

LIST OF FIGURES

CHAPTER 1

INTRODUCTION

The study of quantum degenerate molecular gases is a vibrant field of research, lying at the crossroads between condensed-matter physics and atomic molecular optical physics. Interest in these molecules is driven by the high level of control they offer researchers, to more precisely study a wide range of interactions and chemical processes [1–4]. To reach the quantum degenerate regime, these molecular gases must be cooled to ultracold temperatures, typically on the order of 100 nanoKelvins [5, 6], which has so far been experimentally difficult to achieve [7–10].

As a result, experiments have turned to photoassociation [11] and magnetoassociation [12] as shortcuts to form ultracold molecules from already ultracold atoms. Quantum degenerate molecules have been produced [13–17], but not on a regular basis, and broadening the available methods, and making methods available to systems that are not otherwise accessible [18, 19] continue to move the field forward. Furthermore, obstacles to condensate formation, for instance strong collisions [20], require further study to develop schemes robust enough to overcome these limitations. As the techniques to create quantum degenerate molecules become more robust and experimentally accessible, the creation of colder, larger, and more long-lived samples will open the door to new applications for these molecules. In addition, expanding the conditions under which photoassociation and magnetoassociation are effective could potentially blaze a trail to more complex molecular configurations, such as Efimov trimers [21–23], alkali-earth dimers [18, 19], and molecular ions [24]. The primary focus of this thesis will be to theoretically investigate ways to enhance the combined photoassociation and magnetoassociation techniques to create populations of quantum degenerate molecules more efficiently, and under more realistic and restrictive conditions.

Quantum degenerate molecules are of interest for a number of reasons. Their large dipole moments and long range dipole-dipole interactions [25] make them ideal systems for implementing quantum computation schemes [26,27] and studying macroscopic quantum behavior such as coherent oscillations [28, 29]. Quantum degenerate molecules have opened up a new field of ultracold chemistry [1], allowing researchers to directly study the role of fine and hyper-fine interactions in chemical reactivity [3], chemical reactions in reduced dimensions [4], and even provide information on chemical dynamics at higher temperatures. Since quantum degeneracy allows for tighter constraints and precise spectroscopic determination of physical constants, ultracold molecules could test the limits of the standard model, allowing for an independent confirmation of astrophysical measurements [30]. Additionally, coupled atom-molecule systems have possible applications for creating a macroscopic superposition to determine the upper limit for quantum characteristics [31–34] and as quantum gravity analogs [35]. As quantum degenerate molecules become easier to produce in the laboratory, their potential applications are likely to drive advances in our understanding of fundamental physics for decades to come.

The most prevalent technique, magnetoassociation, was first proposed as a means of creating a BEC of molecules around the turn of the century [36–38]. Also referred to as a Feshbach resonance, magnetoassociation occurs when one atom in a colliding pair spin flips in the presence of a magnetic field tuned near a collision resonance, creating a molecule. The first experiments that successfully created molecules via magnetoassociation were reported in 2003 by multiple groups [39–42]. Subsequently, quantum degeneracy has been achieved on short time scales using magnetoassociation [16].

In an analogous collisional process, photoassociation occurs when a pair of colliding atoms absorbs a photon to create a molecule. Theoretical studies on photoasso-

ciation of ultracold [43–45] and quantum degenerate molecules [46–48] have developed rapidly over the last few decades. The first experiments to create molecules at ultracold temperatures ($T < 1$ mK) using photoassociation were in 1993 on Na [49] and Rb [50], soon followed by other alkali metals [51–53]. Subsequently, experiments have photoassociated heteronuclear molecules [54], including alkali-earth molecules [55] and molecules consisting of different isotopes [56], all in the ultracold regime, and quantum degeneracy ($T < \mu$K) has also subsequently been achieved [13–15].

Molecules formed by photoassociation are electronically excited, and can spontaneously decay to lower levels. To create stable molecules, an additional laser is required to drive the excited molecules into a specific ground state, resulting in a two-color photoassociation process. These two-color processes can be divided into three distinct types, based on the laser configurations. Lasers with fixed intensity and fixed frequency lead to collective oscillations between atoms and stable molecules similar to Rabi oscillations in quantum optics [29,57,58] and Josephson oscillations in a superconductor [59]. Next, lasers with pulsed intensity and fixed frequency, where a free-bound laser pulse creates excited molecules and then a bound-bound pulse drives them to the ground state. The pulses can also take a counter-intuitive order, known as stimulated Raman adiabatic passage (STIRAP), where the bound-bound laser precedes the free-bound laser, so that the excited state is "dark" [60, 61]. Lastly, lasers with fixed intensity and slowly changing frequency, whereby the system adiabatically follows the ground state as it evolves from atoms into stable molecules. This method is used extensively in magnetoassociation experiments [17, 62–64], but has somehow been overlooked as a means to create stable molecules with photoassociation. Another interesting advance has been using the combination of photoassociation and magnetoassociation to create ground state molecules [17,62]. Studies show that these schemes lead to higher rates of molecular formation [65, 66], making them some of

the most promising avenues yet toward the goal of more routine quantum degenerate molecules.

Although photoassociation and magnetoassociation have led the way to quantum degenerate molecules, further flexibility is necessary to expand the available systems on which these techniques will be effective. For example, the laser intensities necessary for photoassociation may prove insufficient for desired atomic species, vibrational levels, condensate sizes, or temperatures. On the other hand, magnetoassociation relies on the width of the Feshbach resonance, which may not be wide enough for the desired application, or may not be available for the atomic species at all [12]. The question is whether association can be harnessed to create stable molecules on a routine basis. The present focus of this thesis will be on modeling the formation of ultracold molecule production via combined photoassociation and magnetoassociation under realistic limiting conditions, with the goal of maximizing efficiency. Some of the limiting conditions that will be explored include low laser intensity, strong elastic collisions, and weak magnetoassociation. Whereas the proof of principle has been firmly demonstrated, there remains room to improve the overall efficiency of molecule formation, or to find configurations that would be useful in systems that are less than ideal for photoassociation or magnetoassociation to succeed.

1.1 Overview

In Chapter 2, we develop the simple model for our study. To illustrate the model, we focus on photoassociation of a homonuclear Bose-Einstein condensate. We define the Hamiltonian that we use to derive the nonlinear Schrödinger equation that describes association of a condensate. One of the advantages of our approach is that further complications can be added to the system without significantly altering the Hamiltonian of the model. We then develop a solution by applying a recursive predictor-corrector algorithm that accounts for the inherent non-linearity

of the system, and reduces the error at each time step by over an order of magnitude [67,68]. Finally, we incorporate a quasicontinuum of non-condensate dissociated atom pairs [69], which provides the beginning of a more realistic model.

In Chapter 3, we investigate the role of spontaneous decay of molecules on the photoassociation rate of a condensate. Once photoassociation of an atomic condensate was proposed as a shortcut to creating a molecular condensate, the question arose whether a fundamental rate limit on atom-molecule conversion exists [14,65,68]. Simply put, the rate limit is set by the time scale for re-filling the atom-pair wave function depleted by strong photoassociation, and this is determined by the inter-particle spacing. In a many-body model, the condensate density sets the inter-particle spacing ($\rho^{-1/3}$), and in a unitary model, the De Broglie wavelength (Λ_D) sets the spacing. This leaves the correct length scale unconfirmed, especially in the deeply quantum degenerate regime. However, the quantum-optics model of strong photoassociation does not currently include spontaneous decay, and the thesis will therefore adapt this model to include spontaneous decay and re-visit the rate limit for atom-molecule conversion [70].

We find that an unanticipated shift in light frequency leads to a maximum in the numerical photoassociation loss rate for strong atom-molecule coupling, similarly to the original many-body model without spontaneous decay [68]. Accounting for the light shift leads to saturation of the numerical rate at about $9\omega_\rho$, so that the many-body rate constant for resonant photoassociation scales with density as $K \propto \rho^{-1/3}$. This limit holds for over two decades of density, where previous analytical results [71, 72] predict this density dependence for limited densities only. The numerical rate agrees with the rate limit obtained for combined photoassociation and Feshbach resonances [73], and we find the many-body rate limit to be generally more strict than a two-body unitary rate limit.

In Chapter 4, we investigate stable molecule formation using two-photon photoassociation by adiabatically sweeping the laser frequencies [74]. In addition to spontaneous decay included in Chapter 3, the thesis will adapt the model to include the addition of a second laser to drive transitions to the ground molecular state, as well as collisions between the particles. Creating stable molecules requires a two-step Raman laser configuration, wherein photoassociation "pumps" atomic population into the electronically-excited molecular state, and a second laser dumps that population into the ground molecular state [75]. However, mostly high laser intensity is required to overcome collisions in the first step, and subsequent strong photodissociation limits creation of molecular condensate.

We focus on adiabatic following, where the ground state of the system "follows" along from atoms to molecules or vice versa, depending on the direction, which is executed by slowly changing the laser frequencies. Using this model, we investigate the feasibility of adiabatic following in low-intensity Raman photoassociation against strong collisions. We also investigate two possible schemes, a two-laser configuration and a four-laser configuration. In the two-laser scheme, stable molecules are coupled to the ground state atoms through an electronically excited state, while in the four-laser scheme, transitions to stable molecules occur through an intermediate, vibrationally excited molecular state in the ground electronic manifold.

Using a model based on a joint Li-Na system, we find that adiabatic following is a viable means for creating a quantum degenerate gas of stable molecules at practical laser intensities and against strong collisions. Transitions directly to the stable molecular state require the least photoassociation intensity, about 30 W/cm^2, and are thus more feasible than transitions via an intermediate state. Collisions cause a DC bias in the frequency, so efficient low-intensity conversion is robust against reasonable increases in the elastic s-wave collision strength. Starting the sweep above

resonance means photodissociation is energetically forbidden once resonance is crossed and molecules begin to form. Since requisite intensity decreases for heavier particles ($I \propto 1/\mu$) [69,74], the method should be feasible for heavier species, heteronuclear or homonuclear, and most likely for other statistics as well.

In Chapter 5, we investigate creating stable molecules through Feshbach-enhanced Raman photoassociation [76]. Building on the model from the previous chapter for two-photon photoassociation, we couple the system to a Feshbach state using strong magnetoassociation, and go from varying the frequency to varying the intensity. Another possible way to mitigate the need for high intensity lasers in Raman photoassociation is to incorporate magnetoassociation. Previous research had shown that strong magnetoassociation can enhance photoassociation [66, 77, 78], due to quantum interference between direct photoassociation and photoassociation via the Feshbach state [73, 79], but whether or not this enhancement would carry over to two-color Raman photoassociation was unclear.

Focusing on pulsed lasers, converting atoms into stable molecules boils down to pulse ordering: the intuitive scheme, where the pump laser turns on first, as opposed to the counterintuitive scheme, where the dump laser turns on first. Whereas the counterintuitive scheme can transfer population to the target state with near-unit efficiency [80], it actually breaks down for an even number of levels [81, 82]. Here we have an even number of levels (atom, Feshbach, excited and stable molecules), but it is possible that the dissociation continuum will act as an effective level, as it has on a separate occasion [68]. We look at both the quasicontinuum model [48, 83], and a resonant-interaction model [65,73,79,84,85], where the Feshbach resonance effectively modifies the photoassociation interaction and laser frequency.

Our results show that strong magnetoassociation can substantially improve photoassociation at low intensities, independent of pulse ordering, but not at high

intensities. The lack of Feshbach enhancement at high intensity is attributed to an already-saturated atom-molecule transition, and the independence of pulse ordering to an unoptimized pulse length for the counterintuitive pulse order. In the quasi-continuum model, vicarious photoassociation losses from the atomic state mean that peak enhancement occurs when the Feshbach frequency is large compared to the photoassociation line width. In the resonant-interaction model, peak enhancement occurs where the resonant inter-atomic interaction vanishes. Disagreement between the resonant-interaction and quasicontinuum models on final conversion efficiencies and the nature of the dark state highlights the importance of explicitly including the Feshbach molecular state in modeling magnetoassociation. Finally, whereas the peak conversion efficiency decreases for stronger intra-atomic, molecular, and atom-molecule collisions, we find that the peak conversion efficiency actually increases for stronger inter-atomic collisions. Systems with a combination of a strong magnetoassociation and strong inter-atomic collisions will therefore be of greater experimental utility, compared to those with a strong magnetoassociation and weak inter-atomic collisions.

In Chapter 6, we investigate creating stable molecules in the case of both weak photoassociation and weak magnetoassociation with assistance from a bound-bound laser coupled to the Feshbach state. In the previous chapter we found that strong magnetoassociation improved molecular conversion of photoassociation at low laser intensity. The question then is whether weak magnetoassociation is capable of enhancing photoassociation in place of strong magnetoassociation. This would open the door to far more experimental capabilities, since the excited state leaks at a much faster rate than Feshbach molecules. Enabling more efficient molecule production using weak association would facilitate studies into species without a strong Feshbach resonance, transitions with poor Frank-Condon overlap, and more

deeply-bound levels. The strong coupling nature of magnetoassociation needs to be replaced, however.

We replicate the effect of strong association by coupling an assisting laser between the Feshbach state and a bound-bound excited state, which has been shown to enhance magnetoassociation [86, 87]. Since it relies on a bound-bound transition rather than a free-bound transition [80], the assisting laser is therefore cheaper and more flexible than either strong magnetoassociation or photoassociation. The question then is whether or not the assisting laser will enhance weak magnetoassociation. The thesis will therefore build on the Chapter 5 model by coupling a laser between the Feshbach state and an additionally-excited molecular state, and thereby investigate Feshbach-enhancement of low intensity Raman photoassociation with a weak magnetoassociation coupling rather than strong.

We find that adding a bound-bound laser in the case of weak magnetoassociation and weak photoassociation can improve the efficiency of ground state molecule conversion. The most improvement in efficiency is observed for the strongest collision strength tested, where the laser-assisted system is twice as effective as Feshbach-enhanced photoassociation, converting 50% stable molecules compared to 20%. Furthermore, as this study was based on light molecules at low density, this efficiency should hold for heavier species, heteronuclear molecules, and higher densities as well. Consequently, this study is proof of principle that the enhanced system offers more flexibility to optimize the experimental setup based on whatever resource is more readily available, while still remaining highly efficient vs. realistic limiting factors.

Finally, Chapter 7 presents an overall conclusion to our findings and the possible directions of further research.

CHAPTER 2

SIMPLE MODEL

In this chapter, we describe the model used to investigate photoassociation and magnetoassociation. Using a simplified model, we demonstrate the numerical components we use to produce our results, which consist of a recursive algorithm to solve the equations of motion, and a predictor-corrector step to account for the nonlinearity. Finally, we demonstrate the advantages of this model by introducing a slightly more complex model.

To understand the theoretical approach used for these investigations, it is useful to begin with a simplified model that demonstrates the basic method that only involves the key characteristics of photoassociation. We focus on photoassociation of a homonuclear Bose-Einstein condensate. We assume that $N \gg 1$ atoms have Bose condensed into the zero momentum state $|a\rangle$, and a laser couples these atoms to zero momentum molecules in the state $|b\rangle$ (Fig. 2.1) so that, in the simplest model, the condensates can be approximated as a two-body system. In second-quantized notation, the Hamiltonian for this system is [69]

$$\frac{H}{\hbar} = \nu b^\dagger b - \frac{1}{2}\Omega(b^\dagger a a + a^\dagger a^\dagger b), \tag{2.1}$$

where $a(b)$ and $a^\dagger(b^\dagger)$ represent the annihilation and creation operators for atoms (molecules), respectively. Ω is the atom-molecule coupling, and ν is the detuning of the photoassociation laser, or the difference between the energy of a photon and the energy required to bind the atoms into a molecule. The annihilation and creation operators follow the commutation relations for bosons, so that $[a, a^\dagger] = 1$, $[b, b^\dagger] = 1$, and all other operators commute. This Hamiltonian is analogous to the Hamiltonian used to model second harmonic generation in quantum optics [88, 89].

We derive equations of motion for the model by taking a mean-field approach,

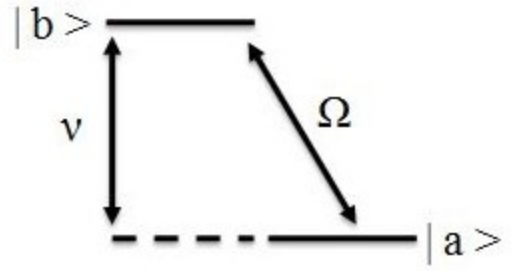

Figure 2.1: Basic 2-level model for photoassociation. $|a>$ and $|b>$ represent atoms and molecules, respectively.

where we make two approximations. First, that the condensates can be described by a single quantum mechanical wave function, and that all bosonic operators can be taken as c-number operators [69] ($a^\dagger(b^\dagger) = a^*(b^*)$). Using the Heisenberg equation, $i\hbar\dot{x} = [x, H]$, where x is the relevant operator, the equations of motion are

$$i\dot{a} = -\Omega a^* b, \tag{2.2a}$$

$$i\dot{b} = \nu b - \frac{1}{2}\Omega a^2, \tag{2.2b}$$

where a is the atomic amplitude and b is the molecular amplitude. Being that this system is the simplest model, yet still including the relevant physics, we use this model to demonstrate the numerical approach to solving the system.

2.1 Numerical Solution

To obtain a numerical solution, we begin by rewriting Eqs. 2.2 in matrix notation

$$i\hbar \begin{pmatrix} \dot{a} \\ \dot{b} \end{pmatrix} = \begin{pmatrix} 0 & -\Omega a^* \\ -\frac{1}{2}\Omega a & \nu \end{pmatrix} \begin{pmatrix} a \\ b \end{pmatrix} \tag{2.3}$$

yielding the nonlinear Schrödinger equation

$$i\hbar\dot{\Psi} = \widehat{H}(\Psi)\Psi, \tag{2.4}$$

where Ψ is the wave function

$$\Psi = \begin{pmatrix} a \\ b \end{pmatrix}, \tag{2.5}$$

and $\widehat{H}$ is a Hamiltonian matrix that depends on Ψ.

With the equations of motion in this form, we formulate a numerical solution using a recursive algorithm adapted from the Crank-Nicolson method [67, 90]. If we ignore the Ψ dependence of $\widehat{H}$ for the time being, taking the differential equation

$$\dot{\Psi} = -i\frac{\widehat{H}}{\hbar}\Psi, \tag{2.6}$$

and applying the Crank-Nicolson formula provides the numerical result

$$\frac{\Psi_i - \Psi_{i-1}}{dt} = -\frac{1}{2}\frac{i}{\hbar}\left[\widehat{H}\Psi_i - \widehat{H}\Psi_{i-1}\right]. \tag{2.7}$$

The time evolution of the wave equation has been discretized, so that $\Psi_i = \Psi(t_i)$ in general, with $t_i = idt$ and $\Psi_0 = \Psi(0)$.

Evaluating Eq. 2.7 for Ψ_i results in the recursive formula

$$\Psi_i = \frac{\widehat{I} - i\frac{dt}{2}\frac{\widehat{H}}{\hbar}}{\widehat{I} + i\frac{dt}{2}\frac{\widehat{H}}{\hbar}}\Psi_{i-1}, \tag{2.8}$$

or more simply

$$\Psi_i = M_- M_+^{-1}\Psi_{i-1}, \tag{2.9}$$

where

$$M_\pm = \widehat{I} \pm i\frac{dt}{2}\frac{\widehat{H}}{\hbar}. \tag{2.10}$$

If we introduce another vector $\phi = M_+^{-1}\Psi_{i-1}$, then $M_+\phi = \Psi_{i-1}$. Using this relation, we can solve the function for the next step, so that $\Psi_i = M_-\phi$. Using this formula, we model the evolution of the system for two simple cases in Fig. 2.2.

Fig. 2.2 shows the evolution of the wave function in the cases of (a) resonance $\nu = 0$, and (b) off resonance $\nu = \Omega$. For both graphs, $\Omega = 1$, $\tau = \Omega t$ is a dimensionless time quantity, so both graphs share the same timescale, and $d\tau/\Omega = 0.001$, so the

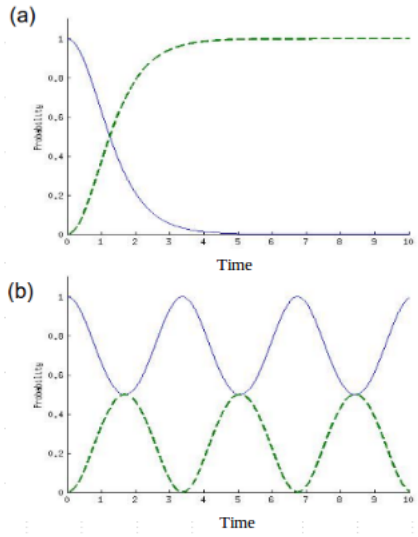

Figure 2.2: Results for 2-Level System in the case of (a) resonance ($\nu = 0$) and (b) off resonance ($\nu = \Omega$). The solid (blue) line represents the wave probability of atoms and the dashed (green) line represents molecular probability, as functions of the dimensionless time τ. Ω is set to 1.

time steps are small enough to ensure convergence. The probabilities are the typical probability amplitudes, $P_A = |a|^2$ and $P_B = 2|b|^2$, where the factor of 2 in P_B arises since one molecule equals 2 atoms. In the case of resonance, the atomic population is fully transferred to the molecular state, and the rate at which this occurs depends on the strength of the photoassociation coupling Ω. In the case of off-resonance photoassociation, the population oscillates between atoms and molecules, analogous to Rabi and Josephson oscillations [29, 57, 59, 91]. The fraction of atoms turned into molecules depends on the detuning, which is a measure of the energy mismatch between atoms and molecules. A larger detuning means more energy mismatch and less population.

In numerical experiments, a quantity that is often used to characterize the photoassociation rate is the time that it takes for the atom condensate probability to drop to $\sim 1/e$, which we call τ_r. The rate is then defined as $R = 1/\tau_r$. Using this measure, we can see how the rate changes, with the results shown in Fig. 2.3.

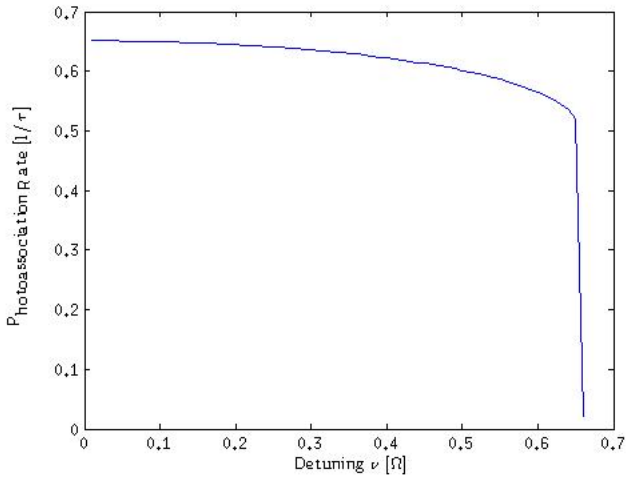

Figure 2.3: Photoassociation rate. The rate is determined by the time it takes for the atomic probability to drop to $1/e$. Quantities are dimensionless, with the rate in units of $1/\tau$ and the detuning in units of Ω, which is set to 1.

Close to resonance, the rate reaches a maximum at about $0.67\Omega^{-1}$. Far from resonance, the rate drops to a vanishingly small rate at a detuning of 0.67Ω, which means this is where the oscillations prohibit the atomic condensate from dropping down to $1/e$. In this region the rate does not exist, since it is presumed on an exponential decay.

To account for the nonlinearity of the system, we adopt a predictor-corrector method, wherein we calculate a predicted solution, and then use this predicted solution to calculate a corrected value. At each time step, we predict a solution $\Psi_i^{predicted}$ according to Eq. 2.8, and we then use this solution to approximate a modified initial vector, $\tilde{\Psi} = [\Psi_i^{predicted} + \Psi_{i-1}]/2$ in $\widehat{H}$. Using this, the reevaluated functions become $\tilde{M}_{\pm} = M_{\pm}(\tilde{\Psi})$ and $\tilde{\phi} = \tilde{M}_{+}^{-1}\Psi_{i-1}$ to obtain a corrected value $\Psi_i^{corrected} = \tilde{M}_{-}\tilde{\phi}$. The corrected value is then taken as the solution for that step, $\Psi_i = \Psi_i^{corrected}$.

To demonstrate the general effects of the nonlinearity, we compare the wave function time evolution according to our model with and without the predictor-corrector step in Fig. 2.4. The first graph shows the atomic probability with a timestep

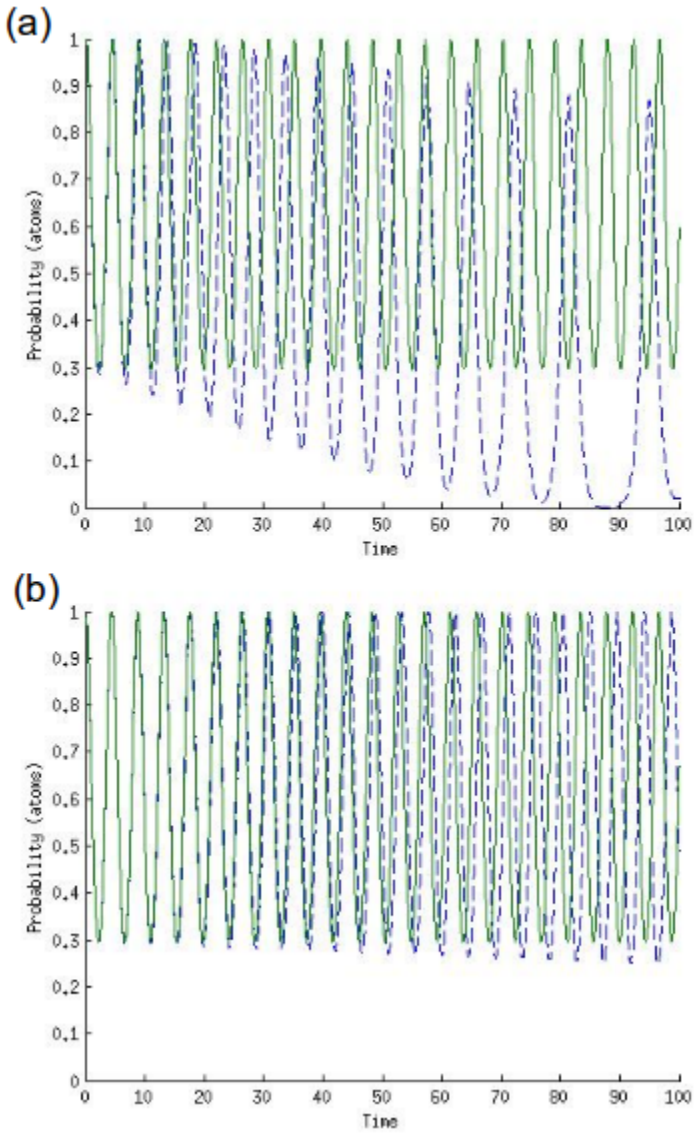

Figure 2.4: Results comparing the numeric model with (solid green lines) and without (dashed blue lines) predictor-corrector step. (a) $d\tau = 0.1$ and (b) $d\tau = 0.01$, with $\Omega = 1$ and $\nu = 0.5$ for both cases. The probability of the atomic condensate is calculated as a function of dimensionless time $\tau = \Omega t$.

of $d\tau = 0.1$, and the second graph with a timestep $d\tau = 0.01$. Since both graphs share the same timescale, (b) requires ten times as many steps to cover the same amount of time. Even though the timestep is relatively large, the predictor-corrector method is already essentially equivalent to previously reported results [68], and to the case with a much smaller timestep, as evidenced by the identical nature of the predictor-

corrector result between (a) and (b). On the other hand, the method without the predictor-corrector shows considerable error accumulation. Even in (b), it still has not converged on the predictor-corrector graph. In other words, at least in this case, the predictor-corrector method was able provide a more accurate model with over an order of 10 times as few time steps compared to without predictor-corrector.

Our numerical model, based on the Crank-Nicholson formula with predictor-corrector, comes with the additional convenience that any further complications can be incorporated into the model without changing the numeric solution or the predictor-corrector algorithm. For example, spontaneous decay and collisions can be added terms within the detuning, while additional states, such as ground state or magnetoassociation molecules, can be added dimensions to Ψ and $\widehat{H}$. To demonstrate these advantages, we now incorporate non-condensate dissociation into the system as an example.

2.2 Photodissociation

Since total momentum is conserved, the atoms with zero momentum will create molecules with zero momentum. However, molecules need not necessarily dissociate back into a pair of atoms with zero momentum, so the model should take this into account [69]. Molecules with zero momentum can photodissociate either back into a pair of condensate atoms in $|a\rangle$, or a pair of non-condensate atoms with equal-and-opposite momentum in the state $|\pm\vec{k}\rangle$ (Fig. 2.5). To account for the non-condensate levels of equal and opposite momentum, the Hamiltonian is modified to read

$$H = \hbar\nu b^\dagger b - \frac{1}{2}\hbar\sum_{\vec{k}}\Omega_k(b^\dagger a_{\vec{k}}a_{-\vec{k}} + a^\dagger_{\vec{k}}a^\dagger_{-\vec{k}}b), \tag{2.11}$$

which shows the interaction now between molecules and two atoms with equal and opposite momenta. The atom-molecule coupling is now $\Omega_k = \Omega f_k$, where f_k contains the momentum-dependence. When $\vec{k} = 0$, $f_k = 1$ and $\Omega_0 = \Omega$, representing the condensate of zero momentum atoms. Using the new Hamiltonian, the Heisenberg

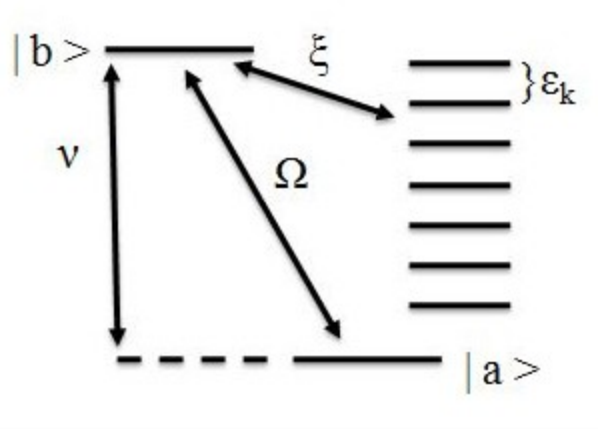

Figure 2.5: Basic model that includes photodissociation. Once atoms are photoassociated into molecules, that can dissociate back into noncondensate pairs, represented by the additional levels coupled through ξ.

equations, and converting the sum over $\vec{k}$ into an integral over ϵ, we derive the new equations of motion

$$i\dot{a} = -\Omega a^* b, \tag{2.12a}$$

$$i\dot{b} = \nu b - \frac{1}{2}\Omega a^2 - \xi \int d\epsilon \sqrt{\epsilon} f(\epsilon) A(\epsilon), \tag{2.12b}$$

$$i\dot{A}(\epsilon) = \epsilon A(\epsilon) - \Omega f(\epsilon) b. \tag{2.12c}$$

Here we define the operator $A(\epsilon) = a_{\vec{k}} a_{-\vec{k}}$, which is the amplitude for dissociated pairs with kinetic energy $\hbar\epsilon = \frac{\hbar^2 \vec{k}^2}{2\mu}$, ξ is the photodissociation coupling between the states $|b\rangle \leftrightarrow |A(\epsilon)\rangle$, and $f(\epsilon)$ contains the energy dependence of the photodissociation coupling.

Before converting Eqs. 2.12 into matrix notation for numerical analysis, the integral over ϵ is converted into a summation over ϵ

$$\int d\epsilon \rightarrow \sum_{i=0}^{n_{QC}} \xi d\epsilon \sqrt{\epsilon_i} f(\epsilon_i) A(\epsilon_i). \tag{2.13}$$

This is done to allow the integral to be evaluated numerically. The matrix notation can be used to approximate the dissociation integral over ϵ by representing it as a quasicontinuum of n_{QC} levels. The number of levels n_{QC} need only be enough so

that the summation numerically represents the integral over a continuous spectrum to within a margin of error. In matrix notation, the nonlinear Schrödinger equation is now

$$i\begin{pmatrix} \dot{b} \\ \dot{a} \\ \dot{A}(\epsilon) \end{pmatrix} = \begin{pmatrix} \nu & -\frac{1}{2}\Omega a & -\sum_i \xi d\epsilon\sqrt{\epsilon_i} f(\epsilon_i) \\ -\Omega a^* & 0 & 0 \\ -\Omega f(\epsilon_i) & 0 & \epsilon_i \end{pmatrix} \begin{pmatrix} b \\ a \\ A(\epsilon_i) \end{pmatrix}, \tag{2.14}$$

where the non-linear Hamiltonian is now

$$\widehat{H} = \begin{pmatrix} \nu & -\frac{1}{2}\Omega a & -\frac{1}{2}\xi d\epsilon\sqrt{\epsilon_1} f(\epsilon_1) & \dots & -\frac{1}{2}\xi d\epsilon\sqrt{\epsilon_{QC}} f(\epsilon_{QC}) \\ -\Omega a^* & 0 & 0 & 0 & 0 \\ -\Omega f(\epsilon_1) & 0 & \epsilon_1 & 0 & 0 \\ \vdots & \vdots & \vdots & \ddots & \vdots \\ -\Omega f(\epsilon_{QC}) & 0 & 0 & 0 & \epsilon_{QC} \end{pmatrix} \tag{2.15}$$

and the wave function is now

$$\Psi = \begin{pmatrix} b \\ a \\ A(\epsilon_1) \\ \vdots \\ A(\epsilon_{QC}) \end{pmatrix}. \tag{2.16}$$

Overall, the numeric solution remains unchanged. In addition, the Hamiltonian matrix remains inherently sparse, up to an arbitrarily large number of dimensions n for the number of condensates n_C and non-condensate levels n_{QC}, where $n = n_C + n_{QC}$. Except along primary horizontal, vertical, and diagonal rows, most of the elements in the matrix remain zero. This sparseness can be utilized to scale calculations proportional to n instead of n^2, significantly conserving computational resources.

CHAPTER 3

THE PHOTOASSOCIATION RATE LIMIT

We begin our study of using association to create quantum degenerate stable molecules by investigating basic characteristics of photoassociation. Photoassociation is a useful shortcut to quantum degeneracy, where a condensate of ultracold molecules is created from a condensate of ultracold atoms [57,92–95], and so should behave quantum mechanically. On the other hand, photoassociation requires two atoms to drift close enough to each other for photoassociation to occur, and the correct length scale for this collision was an open question at the beginning of this dissertation. This offers an interesting test of the wave-particle duality of the condensates, and raises the fundamental question of whether or not a limit on the maximum rate of atom-molecule conversion exists. In a two-body model [96, 97], the De Broglie wavelength Λ_D sets the rate, according to $K = R/\rho \sim \hbar\Lambda_D/\mu$, where K is the density-independent rate constant, R is the photoassociation rate, ρ is the condensate density, and μ is the reduced mass of a dissociated atom pair. This limit is also known as the unitary limit, and at zero temperature depends on the size of the condensate. Conversely, in a many-body model [68], the interparticle spacing determines the rate, and the maximum rate per unit density is approximately $K = R/\rho \sim \hbar\rho^{-1/3}/\mu$. Like the unitary rate, the many-body rate is expected to reach a maximum for strong atom-molecule coupling, and previous numeric results indicated a maximum rate of $\sim 6\omega_\rho$ [68], where ω_ρ is the characteristic frequency of the condensate. This model, however, did not take spontaneous decay into account, and a final answer should include this important physics.

Experiments above [98] or at [15] the quantum degenerate limit have studied the rate limit, and the two limits should merge at the onset of quantum degeneracy, since $1/\rho \sim \Lambda_D^3$, however the deeply degenerate regime has yet to be fully tested for

association. The first experiments with a condensate were thwarted by strong dipole forces at strong laser intensity [14]. Subsequent condensate experiments combined photoassociation and the Feshbach resonance, which enhances photoassociation, and thereby allowed for observation of the rate limit at manageable intensities [65]; these were again consistent with both the many-body [68] and the unitary model [79], and a definitive answer remained elusive. Recent theory [73] has shown that, up to an interference factor, the many-body result for Feshbach-photoassociation agrees reasonably well with the result for photoassociation alone, but agrees with the unitary limit only in a small magnetic-field window near the Feshbach resonance and is otherwise more strict.

Based on an upgrade of the original many-body model [68] of photoassociation that includes spontaneous decay, we investigated the photoassociation rate limit of a Bose-Einstein condensate at zero temperature [70]. The model we use to study the rate limit matches the model introduced in Ch. 2 Sec. 2 with the additional complications of spontaneous decay and heteronuclear photoassociation [99–101], as opposed to simply homonuclear. Numerical experiments reveal an unanticipated light shift in the position of the laser resonance, and the effect of this light shift on the photoassociation rate is examined for high and low condensate densities. Using Li-Na as an example, we find general agreement between numerical results and analytical results, and expect that these results should apply to heavier species, homonuclear pairs, and the analogous Feshbach resonance.

3.1 Many-Body Model with Spontaneous Decay

Consider two miscible Bose-Einstein condensates of atoms [102–104] with N_1 atoms of mass m_1 and N_2 atoms of mass m_2. Photoassociation generally occurs on a time scale much shorter than the timescale for the dipole-dipole and trap interactions, and these are therefore neglected. The atoms are all assumed to be in the zero-

momentum state $|a_1, a_2\rangle = |0_1\rangle\ |0_2\rangle$, with the total number of atoms $N = N_1 + N_2$. The photoassociation laser destroys an atom from each species and creates a dipolar molecule of mass $m_3 = m_1 + m_2$ in the electronically excited state $|e\rangle$, with the laser detuning $\delta_0 > 0$ indicating an open dissociation channel, as per Fig. 3.1(a). In operator notation, the annihilation of an atom (molecule) from an atomic (molecular) condensate is represented by $a_{i,0} \equiv a_i (b_0 \equiv b)$. In the simplest model, only three levels or modes are accessible, and molecules can only dissociate back into the original atomic condensates. To complete our model, we include molecular dissociation to non-condensate levels, as per Fig. 3.1(b). As long as total momentum is conserved, a condensate molecule need not dissociate back to the atomic condensate, but can just as well dissociate into a pair of atoms with equal and opposite momentum. This so-called rogue [68, 71, 72] or unwanted [105, 106] dissociation to non-condensate modes therefore introduces the operators $a_{i,\pm\vec{k}}$. The Hamiltonian for this system is

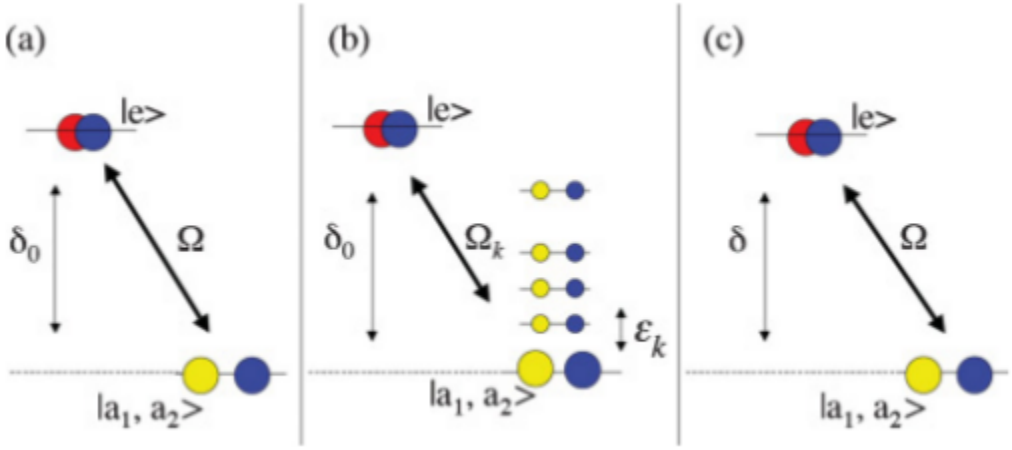

Figure 3.1: Few-level illustration for heteronuclear photoassociation. (a) Basic free-bound transition from the joint condensate to the electronically excited molecular state, where δ_0 is the laser detuning from resonance and Ω is the atom-molecule coupling. (b) Quasicontinuum levels account for photodissociation to atom pairs with equal and opposite momentum, where $\Omega_k = \Omega f_k$. (c) For steady-state photodissociation, the system is effectively a two-level system with a light-shifted detuning δ.

$$\frac{H}{\hbar} = (\delta_0 - i\frac{1}{2}\Gamma_0)b^\dagger b - \frac{1}{2}\sum_{\vec{k}} \Omega_k (b^\dagger a_{1,\vec{k}} a_{2,-\vec{k}} + a^\dagger_{1,\vec{k}} a^\dagger_{2,-\vec{k}} b), \tag{3.1}$$

where Ω is the atom-molecule coupling, δ_0 is the detuning of the photoassociation laser from the $|a_1, a_2\rangle \leftrightarrow |e\rangle$ transition, and Γ_0 is the spontaneous decay strength from the electronically excited molecular state.

To obtain mean-field equations [69], we apply the Heisenberg equation of motion for a given operator, $i\hbar\dot{x} = [x, H]$, where x is the relevant operator, and the operators are then declared c-numbers. We define an operator for the anomalous density, $A_{\vec{k}} = a_{1,-\vec{k}} a_{2,\vec{k}}$, which arises from the non-condensate dissociation. The summation over $\vec{k}$ implicit to the Hamiltonian is then converted to an integral over frequency, introducing the frequency $\omega_\rho = \hbar\rho^{2/3}/\mu$, with $\mu = m_1 m_2/(m_1 + m_2)$ the reduced mass of the atom pair. All told, the mean-field equations of motion are

$$i\dot{a}_1 = -\frac{1}{2}\Omega a_2^* b \tag{3.2a}$$

$$i\dot{a}_2 = -\frac{1}{2}\Omega a_1^* b \tag{3.2b}$$

$$i\dot{b} = \left(\delta_0 - \frac{1}{2}i\Gamma_0\right) b - \frac{1}{2}\Omega a_1 a_2 - \frac{1}{2}\xi \int d\epsilon \sqrt{\epsilon} f(\epsilon) A(\epsilon) \tag{3.2c}$$

$$i\dot{A}(\epsilon) = \epsilon A(\epsilon) - \frac{1}{2}\Omega f(\epsilon) b \tag{3.2d}$$

A microscopic fraction of molecules means that Bose enhancement of spontaneous molecular decay [107] is negligible. Dissociation is treated discretely in terms of the kinetic energy of the atom pair $\hbar\epsilon$, the coupling $4\pi\xi = \Omega/\omega_\rho^{3/2}$, and the continuum shape $f(\epsilon)$. For the sake of numerical convergence, we use a Gaussian for the continuum shape, which takes the form $f(\epsilon) = e^{\frac{\epsilon^2}{2\beta^2}}$, where the width β is set by the semi-classical size of the molecular state, L_0, according to $\beta = \hbar/(2\mu L_0^2)$.

3.2 Results

We develop a simple analytical result for the atom-molecule conversion rate, similar to the approach used in Refs. [79] and [73]. Beginning from Eqs. 3.2, we use

the approximation $\dot{A} = 0$ to adiabatically eliminate A from our system, with the equations of motion becoming

$$i\dot{a}_1 = -\frac{1}{2}\Omega a_2^* b, \tag{3.3a}$$

$$i\dot{a}_2 = -\frac{1}{2}\Omega a_1^* b, \tag{3.3b}$$

$$i\dot{b} = \left(\delta - \frac{1}{2}i\Gamma\right) b - \frac{1}{2}\Omega a_1 a_2, \tag{3.3c}$$

which leaves us with an effectively light shifted few-level system, as per Fig. 3.1(c), where the detuning and damping are now $\delta = \delta_0 + \sigma_0$ and $\Gamma + \Gamma_0 + \gamma_0$, respectively. The light shift $\sigma_0 = \Re(\Sigma)$ and the photodissociation rate $\gamma_0 = \Im(\Sigma)$, where

$$\Sigma = \lim_{\omega \to 0} \left[\frac{1}{4}\Omega\xi \int d\epsilon \sqrt{\epsilon} \frac{f^2(\epsilon)}{\epsilon - \omega} \right]. \tag{3.4}$$

From here, we approximate $\dot{b} = 0$ in a similar manner to eliminate b. This produces all-atom equations of motion with a tunable interaction,

$$i\dot{a}_1 = -\frac{\Omega^2}{4\tilde{\delta}}|a_2|^2 a_1, \tag{3.5a}$$

$$i\dot{a}_2 = -\frac{\Omega^2}{4\tilde{\delta}}|a_1|^2 a_2, \tag{3.5b}$$

where $\tilde{\delta} = \delta - i\Gamma/2$ which defines the (complex) resonant scattering length,

$$\rho^{1/3} a_{res} = -\frac{\Omega^2}{16\pi\omega_\rho(\delta - i\Gamma/2)}. \tag{3.6}$$

The analytical rate for two-body losses from the condensate due to heteronuclear photoassociation becomes

$$R_A = \frac{1}{2}\rho K_A = 4\pi\frac{\hbar\rho}{\mu}\mathrm{Im}(a_{res}), \tag{3.7}$$

where K_A is the rate per unit density, that is, the rate coefficient. The factor of two accounts for the two atomic condensates, whereas ρ is the total density.

In numerical experiments, the rate is determined from the time τ required for

the atomic probability to decay to $\sim 1/e$,

$$R_N = \frac{1}{2}\rho K_N = \frac{1}{\tau}, \tag{3.8}$$

For concreteness, we focus on photoassociation of a joint Li-Na condensate. The atom-molecule coupling is borrowed from photoassociation of ^{7}Li alone [79], so that $\Omega = \Omega_0\sqrt{\rho/\rho_0}$ with $\Omega_0 = 290 \times 2\pi$ kHz and $\rho_0 = 4 \times 10^{12}$ cm^{-3}. We also borrow the semi-classical size of the molecular state $L = 133a_0$, which sets the width of the Gaussian $f(\epsilon)$, and $\Gamma_0 = 12 \times 2\pi$ MHz, the natural linewidth of the excited state.

Results are shown in Figs. 3.2(a) and (c) for $\rho = 10^{14}$ cm^{-3} and in Figs. 3.2(b) and (d) for $\rho = 10^{12}$ cm^{-3}. For lasers tuned to the usual light-shifted resonance [108–111], $\delta_0 = -\sigma$, the numerical rate maximizes at a critical atom-molecule coupling Ω_c [Fig. 3.2; dashed (green) lines], at a value that increases with decreasing density, $R_{max} \sim 4\omega_\rho$ for $\rho = 10^{14}$ cm^{-3} and $R_{max} \sim 5\omega_\rho$ for $\rho = 10^{12}$ cm^{-3}. This density

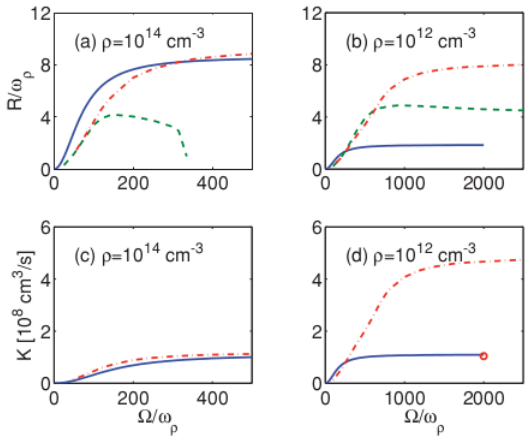

Figure 3.2: Many-body rate limit for heteronuclear photoassociation of a joint Li-Na condensate. (a,b) The solid (blue) line is the analytical rate, and the dashed (green) and dot-dashed (red) lines are the numerical rate without and with the unanticipated light shift, respectively. (c,d) Photoassociation rate constant $K = R/\rho$, where the solid (blue) and dot-dashed (red) lines are, again, the analytical and the light-shifted numerical results, respectively. The open (red) circle in (d) is given by $K_o = K_{max}/(\rho_h/\rho_l)^{1/3}$, where K_{max} is the rate constant for $\rho_l = 10^{12}$ cm^{-3} and $\rho_h = 10^{14}$ cm^{-3}.

dependence is similar to that in Ref. [68], which includes the light shift σ_0.

Moreover, the corrected numerical rate saturates at a value that increases slightly for increasing density, $R_{max}/\omega_\rho = 8.2$ for $\rho = 10^{12}$ cm^{-3} and $R_{max}/\omega_\rho = 8.8$ for $\rho = 10^{14}$ cm^{-3}, in contrast to the unshifted result and Ref. [68]. The rate constant scales with density as $K \propto \rho^{-1/3}$, as indicated by the open (red) circle in Fig. 3.2(b). Also, the analytical results [solid (blue) line] agree best with the numerical results for high density. Finally, R/ω_ρ depends very weakly on density, so that inhomogeneous effects, which we have neglected, should be marginal.

To find the unanticipated light shift, we began with a detuning with the initial expected light shift $\delta = \sigma_0$. We then changed the detuning incrementally so that τ is minimized. We found an unanticipated light shift of the form

$$\sigma_u = 1.2 \left(\frac{\Omega}{\Omega_c} \right)^2 \Gamma_0, \tag{3.9}$$

where $\sigma = \sigma_0 + \sigma_u$. Including σ_u leads to saturation instead of maximization [Fig. 3.2; dot-dashed (red) lines].

The detuning light shift is shown in Fig. 3.3. At photoassociation couplings

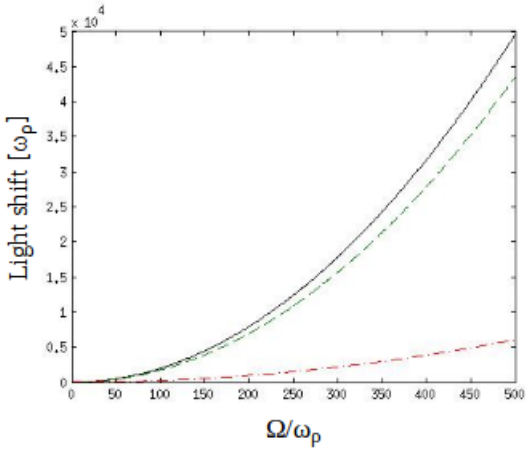

Figure 3.3: Detuning light shift for $\rho = 10^{14}$ cm^{-3}. The solid (black) line is the total light shift σ, the dashed (green) line is the expected light shift due to dissociation σ_0, and the dot-dashed (red) line is the unanticipated light shift).

below the saturation region, the deviation from resonance accounted for by the unanticipated shift is small compared to the overall shift. On the other hand, since both the expected light shift σ_0 and the unexpected light shift σ_u increase proportional to Ω^2, this means $\sigma_0 \propto \sigma_u$. So even though the unanticipated shift grows as the photoassociation coupling increases, its overall contribution to the shift remains proportionally the same. Nevertheless, neglecting this shift makes a significant difference in the rate limit, as Fig. 3.2 shows, since photoassociation is most effective close to light-shifted resonance.

Without the light shift, the effective detuning away from resonance is larger, which hampers photoassociation into bound state molecules. This effect is shown in Fig. 3.4, which shows the conversion of the probability of atoms into dissociated pairs (a) without and (b) with the unanticipated light shift in the just saturated regime. The atomic probability is calculated as $P_A = |a_1|^2 + |a_2|^2$, and the probability of dissociated pairs is $P_D = \int d\epsilon \sqrt{\epsilon} A(\epsilon)/4\pi^2\omega_\rho^{3/2}$. The probability of excited molecules remains minuscule and are thus neglected from the figures.

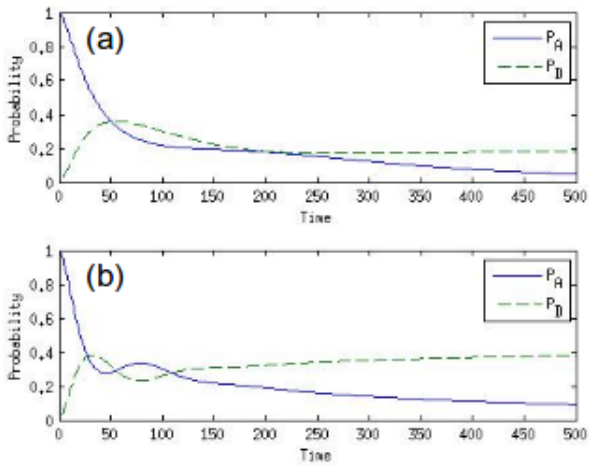

Figure 3.4: Probability evolution (a) without and (b) with the unanticipated light shift at $\Omega/\omega_\rho = 200$. The solid (blue) lines represent the probability of atoms and the dashed (green) lines show the probability of dissociated pairs. $\rho = 1 \times 10^{14}$ cm^{-3}. Time is in the dimensionless quantity $\tau = \Omega t$.

At the coupling strength of 200 ω_ρ at the density $\rho = 1 \times 10^{14}$ cm^{-3}, the unanticipated light shift accounts for a 75% higher photoassociation rate, from 4 ω_ρ to 7 ω_ρ. This can be seen in Fig. 3.4, where P_A drops to $1/e$ in 50τ without the light shift [Fig. 3.4(a)], but it only takes 29τ with the light shift [Fig. 3.4(b)].

The precipitous drop in the numerical rate in Fig. 3.2(a) arises because coherent (Rabi) oscillations are now strong enough to obstruct photoassociation, especially when the system is not on light-shifted resonance. Absent the light shift, the strongly coupled system undergoes Rabi oscillations between atomic condensate and photodissociated pairs [68] before the atomic probability can drop to $1/e$, significantly suppressing the rate constant. Results comparing the effect of the anomalous light shift for this region are shown in Fig. 3.5. Not accounting for the light shift [Fig. 3.5(a)] reduces the photoassociation rate, so that P_A takes 459τ to drop to $1/e$. However, including the light shift [Fig. 3.5(b)] increases the rate at which the atomic probability drops, so that it reaches $1/e$ in 48τ, nearly a tenfold increase. Since the unanticipated shift gets increasingly larger for increasing photoassociation, its suppression of

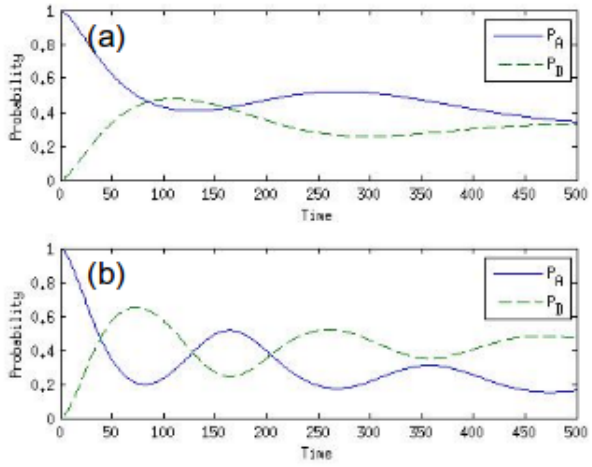

Figure 3.5: Probability evolution (a) without and (b) with unanticipated light shift at $\Omega/\omega_\rho = 400$. The solid (blue) lines represent the probability of atoms and the dashed (green) lines show the probability of dissociated pairs. $\rho = 1 \times 10^{14}$ cm^{-3}. Time is in the dimensionless quantity $\tau = \Omega t$.

the rate, combined with Rabi oscillations, is subsequently magnified.

In Fig. 3.4, collective oscillations between P_A and P_D are suppressed by spontaneous decay, which is the dominant process. In Fig. 3.5, the photoassociation strength ($\Omega = 400\omega_\rho$) is approaching the strength of spontaneous decay ($\Gamma_0 = 593\omega_\rho$), so collective oscillations are again becoming relevant. The rate of the oscillations are faster with the light shift, which is the expected result when the system is closer to resonance.

We also compare the many-body rate to the two-body unitary limit, shown in Fig. 3.6. The unitary limit is set by the De Broglie wavelength of the condensate atoms according to

$$\frac{R_U}{\rho} = K_U = \frac{\hbar}{m}\Lambda_D. \tag{3.10}$$

In the zero-temperature limit, the De Broglie wavelength is given by the mean Thomas-Fermi radius of the condensate

$$\Lambda_D = 2R_{TF} = \sqrt{\frac{8\hbar\mu}{m\bar{\omega}^2}}, \tag{3.11}$$

where $\bar{\omega}^3 = \omega_x\omega_y\omega_z$ defines the mean trapping frequency, and we assume that the

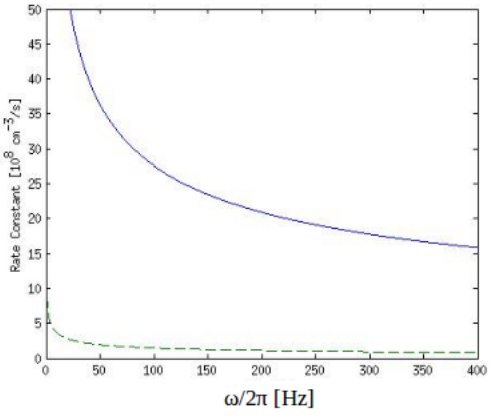

Figure 3.6: Photoassociation rate constant for a Bose-Einstein condensate vs. trap frequency. The solid (blue) line is the unitary-limited rate constant and the dashed (green) line is the many-body rate constant.

frequencies can be adjusted so that the two condensates have identical sizes. The condensate chemical potential is [112]

$$\mu = \frac{1}{2}\bar{\omega}\left(\frac{15Na}{L_{ho}}\right)^{2/5}, \tag{3.12}$$

where N is the number of atoms in the condensate, and $L_{ho} = \sqrt{\hbar/(m\bar{\omega})}$ is the harmonic oscillator length scale. The s-wave scattering length is a and is taken to be the background (zero-field) value, as the expansion of the condensate due to photoassociation is at the same time scale as the motion of the atoms in the trap, which is much longer than the timescale of photoassociation. Results are shown in Fig. 3.6 for trap frequencies satisfying $\sqrt{2}\omega_x = \omega_y = \omega_z/\sqrt{2}$ and $N_i = 10^6$ atoms. For loose traps, that is, low density, the two-body unitary limit set by the condensate size is over an order of magnitude larger than the many-body rate limit.

3.3 Summary

We have investigated the rate limit on photoassociation of a Bose-Einstein condensate, using an upgraded model that explicitly includes spontaneous radiative decay. We found an unanticipated light shift that, once taken into account, produces a maximum numerical photoassociation loss rate for strong atom-molecule coupling that agrees with the many-body model without spontaneous decay [68]. Overlooking this shift qualitatively alters the characteristic result of a rate-limit that saturates and a stricter rate limit that optimizes.

The numerical rate saturates at about $9\omega_\rho$, so that the many-body rate constant for resonant photoassociation scales with density as $K_N \propto \rho^{-1/3}$. This limit holds for over two decades in densities, whereas recent analytical results [71, 72] predict this density dependence for limited densities. This limit also agrees with the rate limit obtained for combined photoassociation and Feshbach resonances [73]. Our analytical approximation yields a rate constant that is independent of density and agrees best with the numerical result for dense condensates. Finally, the many-body rate

limit has been shown explicitly to be generally stricter than a two-body unitary rate limit. Having answered a fundamental question on the rate limit of photoassociation alone, we can turn our attention to creating stable molecules through two-photon photoassociation.

CHAPTER 4

STABLE MOLECULES I: ADIABATIC PASSAGE IN RAMAN PHOTOASSOCIATION

While in the previous chapter, we studied the formation of molecules using one-photon photoassociation, here we study schemes with two or more lasers. Photoassociation creates excited molecules, and at least one other laser is required to drive the molecules into a ground state due to dipole selection rules. These two-photon schemes [113, 114] can take different forms based on the laser characteristics, as discussed in our Introduction. Here we focus on an adiabatic following scheme [93, 115, 116], where the laser intensity remains fixed while the frequency is slowly changed. Although this method is used extensively in magnetoassociation experiments [17,62–64], it has been overlooked in photoassociation experiments. In particular, we look at two schemes: a two-laser scheme, where stable molecules are effectively coupled directly to the atomic state via a two-photon photoassociation transition, and a four-laser scheme, where stable molecules are created through an intermediate, vibrationally excited state. We find that this adiabatic following scheme is a viable method for creating stable molecules using practical laser intensities, that the two-laser scheme is more efficient than the four-laser scheme for manageable intensities, and that this scheme is robust against reasonable increase in the collisional interaction strength [74].

Although atoms can be cooled to the quantum degenerate regime through direct cooling techniques alone [117–119], molecules require the cooling of more degrees of freedom [92], and the direct cooling methods that are effective for atoms have yet to reach sufficiently low temperatures to achieve quantum degeneracy for molecules [7, 120]. Photoassociation is an efficient shortcut that bypasses the need to cool molecules directly; instead, ultracold molecules are formed from already ultracold atoms [92]. In photoassociation, two colliding atoms absorb a photon to create

a bound molecule [97]. The molecule is electronically excited [92], and a second laser is needed to drive the excited molecule into a ground state. We focus on an adiabatic following scheme, where laser intensity is fixed while frequency is slowly changed, and the system adiabatically follows the ground state as it evolves from atoms into stable molecules [93, 115, 116].

Adiabatic following is used extensively in magnetoassociation experiments [17, 62–64], but had been largely overlooked as a means to create stable molecules with photoassociation. According to the adiabatic theorem [121–124], when a system undergoes an adiabatic change after starting in the ground state, then the system will follow the ground state as it evolves under the adiabatic change [125]. Consider a system that consists of atoms and molecules coupled by association, be it photoassociation or magnetoassociation. The system begins in the ground state, either all atoms for large positive laser detuning (Δ), or all molecules for large negative detuning. We then apply an adiabatic change in the detuning from the association resonance, as in Fig. 4.1, where a slow change of the laser detuning from large and positive to large and negative changes the ground state from atoms to molecules. In the other direction, beginning with a large and negative detuning and going to large and positive, the ground state follows from molecules to atoms. This is just the adiabatic theorem in action, whereby the system follows the ground state from atoms to molecules and vice versa.

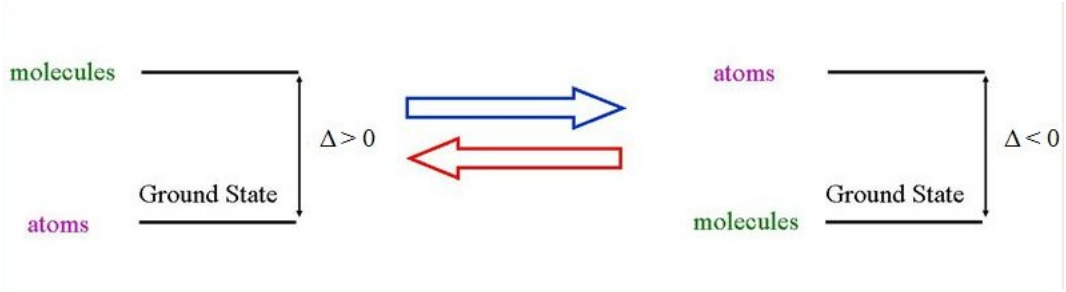

Figure 4.1: Adiabatic Following Diagram.

We study these expected results with an upgraded model, building upon the model from Ch. 3. The model is enhanced to include the addition of multiple lasers to drive transitions to the ground molecular state. Because the lifetimes for stable molecules are much longer than the lifetimes for excited molecules created in one-photon photoassociation that was studied in Ch. 3, we also explicitly include elastic collisions between particles. To model realistic results, we use parameters based on a Li-Na system to measure stable molecule formation, and we also investigate more restrictive conditions such as low intensity lasers and strong collisions.

We find that for practical laser intensities, adiabatic following is a possible method for creating stable molecules. To create stable molecules, the frequency sweep should be started above resonance, in which case photodissociation is energetically forbidden. The two-laser scheme requires the least photoassociation intensity, ~ 30 W/cm^2 for the Li-Na system, and is therefore more feasible than the four-laser scheme with an intermediate, vibrationally excited molecular state, and this intensity decreases for heavier particles. Low-intensity conversion is also robust against reasonable increases in the strength of elastic s-wave collisions, which cause a mean-field shift in the frequency resonance. This method should therefore be applicable to a wide range of systems, including heavier species, heteronuclear or homonuclear systems, and other statistics.

4.1 Two-Laser Scheme

In keeping with Ch. 3, we focus on the creation of dipolar molecules via heteronuclear Raman photoassociation [99–101] as per Fig. 4.2(a). Consider a mixture of two atomic species that have Bose condensed into the state $|a_1, a_2\rangle$. One photoassociation laser converts an atom from each species to an electronically excited molecule in the state $|e\rangle$, where Ω_1 is the atom-molecule coupling and δ is the one-photon detuning, which arises from the energy mismatch between the laser 1 photons

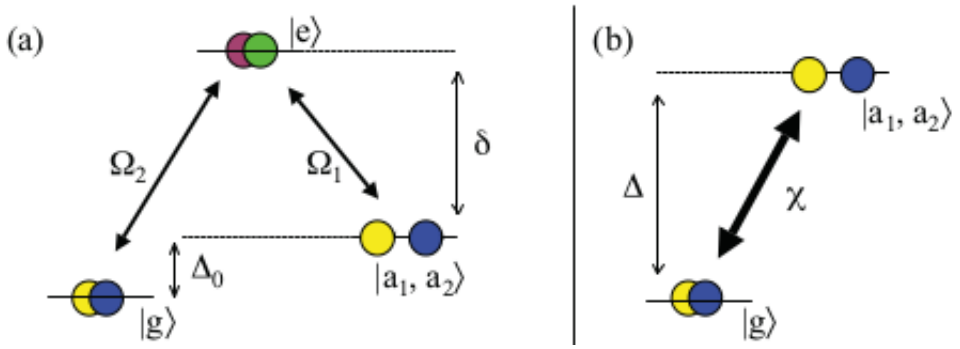

Figure 4.2: Adiabatic Following via Two-Level Scheme. (a) Two-photon photoassociation. (b) When laser 1 is far off resonance, the effect is a two-photon coupling between atoms and stable molecules.

and the energy of the molecular state $|e\rangle$ relative to the atomic state $|a_1, a_2\rangle$. The state $|e\rangle$ undergoes spontaneous radiative decay at the rate Γ_0, as well as stimulated decay, where the molecule dissociates into a pair of atoms with equal and opposite nonzero momentum, and are therefore not part of the original condensate. A second laser converts excited molecules from $|e\rangle$ into stable molecules in the state $|g\rangle$, with Ω_2 the molecule-molecule coupling, and Δ_0, the two-photon detuning that describes the difference between the total energy of the two laser photons and the energy of the molecular state $|g\rangle$ relative to the atomic state $|a_1, a_2\rangle$. Elastic collisions between particles change the relative energy between the states, and therefore the detuning of the lasers, according to the coupling $\Lambda_{ij} \propto \rho a_{ij}/\mu_{ij}$, where ρ is the total particle density, a_{ij} is the s-wave scattering length, and μ_{ij} is the reduced mass for the ith and jth particles.

The mean-field equations of motion for this system are obtained in a similar fashion to Ch. 2 and Ch. 3, and are

$$i\dot{a}_1 = \omega_1 a_1 - \frac{1}{2}\Omega_1 a_2^* b, \tag{4.1a}$$

$$i\dot{a}_2 = \omega_2 a_2 - \frac{1}{2}\Omega_1 a_1^* b, \tag{4.1b}$$

$$i\dot{b} = (\delta - i\frac{1}{2}\Gamma_0)b - \frac{1}{2}\Omega_1 a_1 a_2 - \frac{1}{2}\Omega_2 g - \xi \int d\epsilon \sqrt{\epsilon} f(\epsilon) A(\epsilon), \tag{4.1c}$$

$$i\dot{g} = (\Delta_0 + \omega_3)g - \frac{1}{2}\Omega_2 b, \tag{4.1d}$$

$$i\dot{A}(\epsilon) = \epsilon A(\epsilon) - \frac{1}{2}\Omega_1 f(\epsilon) b. \tag{4.1e}$$

Here $a_{1(2)}$ is the probability amplitude for atomic species 1 (2), b (g) is the amplitude for excited (stable) molecules in the $|e\rangle$ ($|g\rangle$) molecular state, and $A(\epsilon)$ is the amplitude for atom pairs that are photodissociated out of the condensate. $\hbar\epsilon = p^2/2\mu_{12}$ is the kinetic energy of a photodissociated pair, $f(\hbar\epsilon)$ is the energy spectrum of dissociated pairs, and $\xi = \Omega_1/8\pi^2\omega_\rho^{3/2}$ is the photodissociation coupling, where $\omega_\rho = \hbar\rho^{2/3}/2\mu_{12}$. The shifts in the energy levels due to elastic collisions are accounted for by $\omega_1 = \Lambda_{11}|a_1|^2 + \Lambda_{12}|a_2|^2 + \Lambda_{13}|g|^2$, $\omega_2 = \Lambda_{12}|a_1|^2 + \Lambda_{22}|a_2|^2 + \Lambda_{23}|g|^2$, and $\omega_3 = \Lambda_{13}|a_1|^2 + \Lambda_{23}|a_2|^2 + \Lambda_{33}|g|^2$. Trapping of the particles and dipole-dipole interactions are negligible on the time scale for atom-molecule conversion and so are excluded from the model.

When the photoassociation laser is far off resonance with the transition $|a_1, a_2\rangle \leftrightarrow |e\rangle$, i.e., for $|\delta| \gg 0$, then one-photon transitions to the excited state $|e\rangle$ are negligible and two-photon transitions directly to the stable molecular state $|g\rangle$ dominate, as per Fig. 4.2(b). The excited state is thus only ever negligibly populated, and so we have neglected their contribution to collisions. The two-photon coupling between the atoms and stable molecules is $\chi = \Omega_1\Omega_2/2\delta$, the effective two-photon detuning is $\Delta = \Delta_0 - \Omega_2^2/\delta$, and the effective spontaneous decay rate is $\Gamma_1 = (\Omega_2/2\delta)^2\Gamma_0$. The mean-field equations of motion become

$$i\dot{a}_1 = \omega_1 a_1 - \frac{1}{2}\chi a_2^* g, \tag{4.2a}$$

$$i\dot{a}_2 = \omega_2 a_2 - \frac{1}{2}\chi a_1^* g, \tag{4.2b}$$

$$i\dot{g} = (-\Delta + \omega_3 - i\frac{1}{2}\Gamma_1)g - \frac{1}{2}\chi a_1 a_2 - \frac{\chi}{8\pi^2\omega_\rho^{3/2}}\int d\epsilon\sqrt{\epsilon} f(\epsilon) A(\epsilon), \tag{4.2c}$$

$$i\dot{A}(\epsilon) = \epsilon A(\epsilon) - \frac{1}{2}\chi f(\epsilon) g. \tag{4.2d}$$

We refer to this model as the two-level scheme, per the initial condensate atoms and the final stable molecules. The role of photodissociation to noncondensate pairs is expected to be significant when $\chi \gtrsim \omega_\rho$ [68, 72].

4.1.1 Two-Laser Results

Since the required laser intensity for photoassociation decreases for heavier atomic species, we look at the lightest (alkali-metal) heteronuclear molecule Li-Na. The atom-molecule coupling Ω_1 for the $|a_1, a_2\rangle \leftrightarrow |e\rangle$ transition is obtained by scaling a typical Ω_1 for homonuclear photoassociation of ^{7}Li [15, 79], so that $\Omega_1/2\pi = \sqrt{(\mu_0/\mu_{12})(\rho/\rho_0)(I/I_0)} \times 290$ kHz, where $\mu_0 = 3.5$ a.u., $\rho_0 = 4 \times 10^{12}$ cm^{-3}, and $I_0 = 28$ W/cm^2. For $\Gamma_0/2\pi = 12$ MHz, the detuning of the photoassociation laser is set to $\delta = 100\Gamma_0$, which is large enough to suppress spontaneous decay with $\chi = 100\Gamma$ for reasonable intensities but small enough to avoid interference from neighboring states of the photoassociation target $|e\rangle$. The molecule-molecule coupling is set to $\Omega_2 \lesssim \Gamma_0$, which is generally possible for reasonable laser intensity. For dense condensates, $\rho = 10^{14}$ cm^{-3}, the largest coupling for elastic collisions is estimated [20] as $\Lambda_{max} \approx 0.3\omega_\rho$, so that strong with respect to two-photon photodissociation is essentially the same as strong with respect to collisions. As per Table 4.1, we vary the coupling χ from strong to weak (relative to ω_ρ), although only weak coupling corresponds to photoassociation laser intensities that are easily achieved [14, 65].

In general, the detuning Δ represents the difference between the two-photon energy and the relative atom-molecule energy. We can think of Δ as simply the energy

$\chi(\omega_\rho)$	$\Omega_1(\omega_\rho)$	I_1 (W/cm^2)	$\Omega_2(\Gamma_0)$
6.16	602	3.05×10^3	1.02
0.61	191	307	0.324
0.065	62	32.3	0.105

Table 4.1: Estimated Typical Parameters for ^{7}Li-Na.

of the stable molecular state (relative to the atomic state) that is tunable according to the frequency of the lasers. For a laser frequency such that $\Delta > 0$, as in Fig. 4.2(b), the ground state of the system is then stable molecules, whereas the ground state of the system is atoms for $\Delta < 0$. According to the adiabatic theorem [124], if the system begins as atoms above resonance and the laser frequency is adjusted so that Δ changes adiabatically from positive to negative, then the system will follow the ground state as it evolves from atoms to stable molecules. Since the two-photon coupling χ sets the frequency scale, a change of laser frequency is adiabatic if $|\Delta_f - \Delta_i| \lesssim \chi$ for $(t_f - t_i) \lesssim \chi^{-1}$. Hence, we use $\Delta(t) = \Delta_i \pm (\chi^2/10)t$. To maintain the condition that $\delta = 100\Gamma_0$, which mitigates decay, we effect the change in the two-photon detuning Δ by changing the frequency of laser 2, leaving the frequency of laser 1 fixed.

Results of photoassociation via adiabatic following are illustrated for an ideal gas in Figs. 4.3(a)-(c), where solid (dashed) lines are molecules (atom pairs) and initial atoms are not shown. For $\Delta_{initial} < 0$, as discussed above, the system follows the ground state as it evolves from atoms to molecules, independent of the atom-molecule coupling, following the right arrows. Following the left arrows where $\Delta_{initial} > 0$, the system follows the ground state from molecules to atoms. At strong coupling [Fig. 4.3(a)], molecules form near resonance but are quickly lost to photodissociation, since it is energetically favorable for $\Delta < 0$. At weak coupling [Fig. 4.3(c)], photodissociation produces few pairs on the given time scale, so results are independent of the sign of $\Delta_{initial}$.

Adding collisions makes little difference for strong and moderate couplings [Figs. 4.3(d) and 4.3(e)]. For weak photoassociation [Fig. 4.3(f)], collisions produce a shift in the two-photon resonance and lead to an apparent asymmetry with respect to the direction of the detuning change. Atom-molecule conversion takes place largely near resonance within $\Delta \approx \pm\chi/2$, which for weak coupling translates into a rate

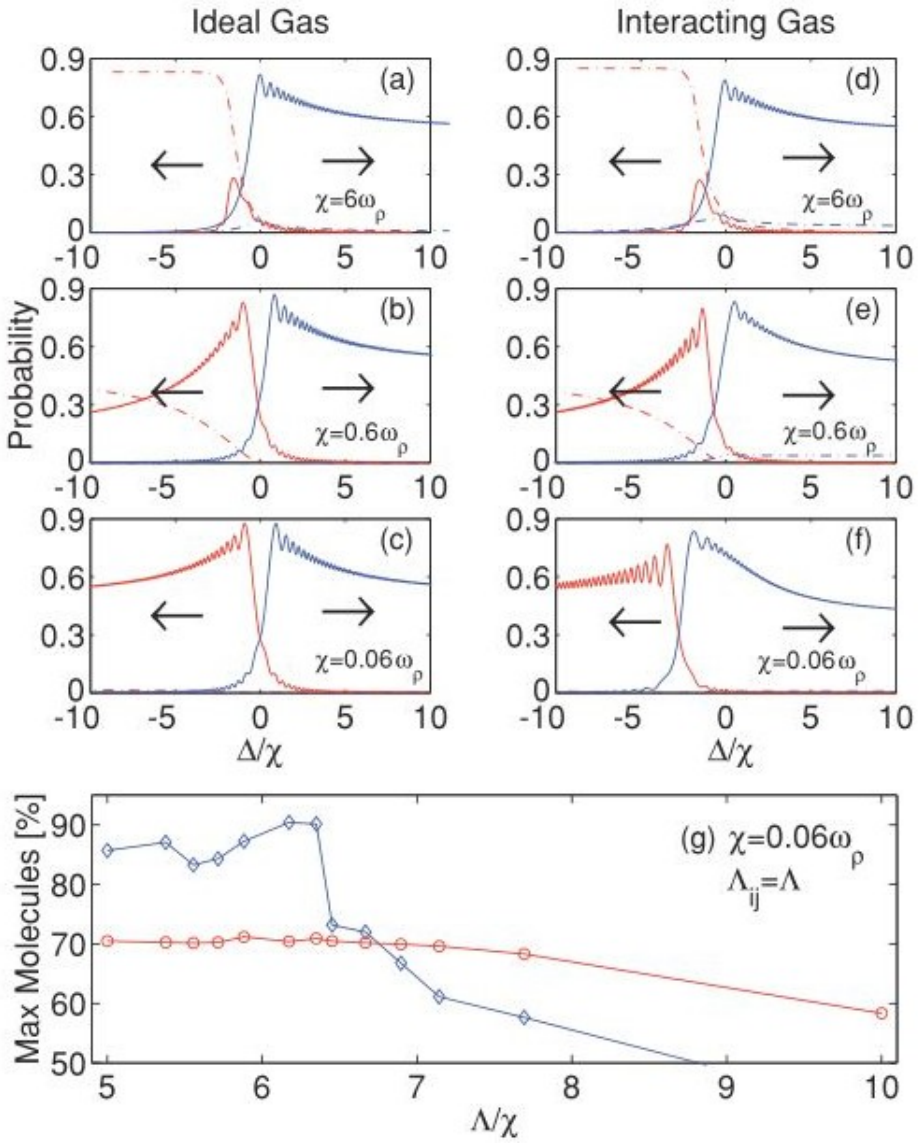

Figure 4.3: Two-laser scheme probability vs. two-photon detuning for ideal gases (a)-(c) and interacting gases (d)-(f) at varying coupling strength χ. Arrows indicate direction of change in Δ over time. Solid lines denote molecules and dashed lines denote dissociated pairs. (g) Maximum molecule percentage at weak coupling and varying collision strength. Blue diamonds (red circles) denote starting below (above) resonance.

$R \approx \chi/10 \ll \omega_\rho$ and a time scale of about 0.5 ms, far below the rate limit [14,65,68,72].

To determine how much collisions can affect the results, we examine stronger collisions by setting $\Lambda_{ij} = \Lambda$ and fixing $\chi = 0.06\omega_\rho$ [Fig. 4.3(g)]. For increasing Λ, the conversion efficiency maximizes for $\Delta_{initial} < 0$, and conversion for $\Delta_{initial} > 0$ is relatively unaffected. Compared to $\Lambda_{max}/\chi \approx 5$ in Fig. 4.3(f), conversion $\sim 90\%$ survives an increase in the strength of elastic collisions $\sim 30\%$. Finally, extrapolating to heavier systems should be possible. Since $\Lambda_{max}/\chi \propto (a_{max}/\mu_{max})\sqrt{\mu_{12}/I_1}$, heavier particles will require less intensity I_1 to satisfy equivalent photoassociation coupling strength relative to s-wave scattering length a_{max} to maintain equivalent molecule conversion, although other considerations may ultimately negate this advantage. Further study is warranted.

4.2 Four-Laser Scheme

We also consider the four-laser scheme illustrated in Fig. 4.4(a), where transitions to stable molecules occur through an intermediate, vibrationally excited molecular state in the ground electronic manifold. The photoassociation laser still converts atom pairs in the state $|a_1, a_2\rangle$ into electronically excited molecules in state $|e_1\rangle$, but

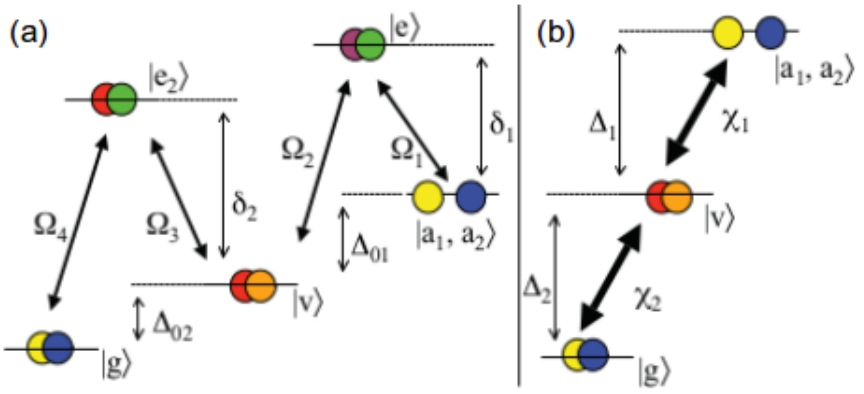

Figure 4.4: Adiabatic Following via Four-Laser Scheme. (a) Four-photon transitions through an intermediate vibrational state. (b) When lasers 1 and 3 are both off resonance, the effect is a three-level system of atoms, vibrationally excited molecules, and vibrationally stable molecules.

the second laser now converts molecules in the state $|e_1\rangle$ into electronically stable, vibrationally excited molecules in state $|v\rangle$. A third laser then converts molecules in $|v\rangle$ into molecules in a second electronically excited state $|e_2\rangle$, and a fourth laser converts molecules in state $|e_2\rangle$ into molecules in the stable state $|g\rangle$. The laser 1 and 2 couplings and detunings are as defined previously, whereas the laser 3 (4) coupling is $\Omega_{3(4)}$, the detuning of laser 3 from the $|v\rangle \leftrightarrow |e_2\rangle$ transition is δ_2, and the detuning of lasers 3 and 4 from the two-photon transition $|v\rangle \leftrightarrow |g\rangle$ is Δ_{02}. Spontaneous decay from the states $|e_1\rangle$ and $|e_2\rangle$ is taken to occur at the same rate Γ_0. The mean-field equations of motion are now

$$i\dot{a}_1 = \omega_1 a_1 - \frac{1}{2}\Omega_1 a_2^* e_1, \tag{4.3a}$$

$$i\dot{a}_2 = \omega_2 a_2 - \frac{1}{2}\Omega_1 a_1^* e_1, \tag{4.3b}$$

$$i\dot{e}_1 = (\delta_1 - i\frac{1}{2}\Gamma_0)e_1 - \frac{1}{2}\Omega_1 a_1 a_2 - \frac{1}{2}\Omega_2 b - \xi \int d\epsilon \sqrt{\epsilon} f(\epsilon) A(\epsilon), \tag{4.3c}$$

$$i\dot{b} = (\Delta_{01} + \omega_3)b - \frac{1}{2}\Omega_2 e_1 - \frac{1}{2}\Omega_3 e_2, \tag{4.3d}$$

$$i\dot{e}_2 = (\delta_2 - i\frac{1}{2}\Gamma_0)e_2 - \frac{1}{2}\Omega_3 b - \frac{1}{2}\Omega_4 g, \tag{4.3e}$$

$$i\dot{g} = (\Delta_{02} + \omega_4)g - \frac{1}{2}\Omega_4 e_2, \tag{4.3f}$$

$$i\dot{A}(\epsilon) = \epsilon A(\epsilon) - \frac{1}{2}\Omega_1 f(\epsilon) e_1. \tag{4.3g}$$

where $e_{1(2)}$ is the amplitude for the molecules in the electronically excited $|e_{1(2)}\rangle$ state, and $b(g)$ is the amplitude for the electronically stable, vibrationally excited (stable) molecular state $|v\rangle$ ($|g\rangle$).

When laser 1 is far off resonant from the transition $|a_1, a_2\rangle \leftrightarrow |e_1\rangle$, and laser 3 is off resonant with the $|v\rangle \leftrightarrow |e_2\rangle$ transition, then two-photon transitions $|a_1, a_2\rangle \leftrightarrow |v\rangle$ and $|v\rangle \leftrightarrow |g\rangle$ will dominate, as illustrated in Fig. 4.4(b). The primary two-photon parameters are the same as Eqs. (4.2), and the secondary two-photon parameters are $\chi_2 = \Omega_3\Omega_4/2\delta_2$, $\Delta_2 = \Delta_{02} + \Omega_4^2/2\delta_2$, and $\Gamma_2 = (\Omega_4^2/2\delta_2)^2\Gamma_0$. Here the frequency of

laser 1 (3) is fixed such that $\delta_{1(2)} = 100\Gamma_0$, so that adiabatic following due to changing $\Delta_{1(2)}$ is effected by changing the frequency of laser 2 (4). The ω_i are again determined by $\Lambda_{ij} \propto \rho a_{ij}$, and collision-induced vibrational relaxation [126] of molecules in $|v\rangle$ is included with imaginary scattering lengths estimated from ^{87}Rb [13, 127]. The resulting mean field equations of the model for the three-level scheme are

$$i\dot{a}_1 = \omega_1 a_1 - \frac{1}{2}\chi_1 a_2^* b, \tag{4.4a}$$

$$i\dot{a}_2 = \omega_2 a_2 - \frac{1}{2}\chi_1 a_1^* b, \tag{4.4b}$$

$$i\dot{b} = (\Delta_1 + \omega_3 - i\frac{1}{2}\Gamma_1)b - \frac{1}{2}\chi_1 a_1 a_2 - \frac{1}{2}\chi_2 g - \frac{\chi_1}{8\pi^2\omega_\rho^{3/2}}\int d\epsilon\sqrt{\epsilon}f(\epsilon)A(\epsilon), \tag{4.4c}$$

$$i\dot{g} = (\Delta_2 + \omega_4 - i\frac{1}{2}\Gamma_2)g - \frac{1}{2}\chi_2 b, \tag{4.4d}$$

$$i\dot{A}(\epsilon) = \epsilon A(\epsilon) - \frac{1}{2}\chi_1 f(\epsilon) b. \tag{4.4e}$$

4.2.1 Four-Laser Results

We now slowly change atoms into stable molecules in two steps, where a slow change in Δ_1 converts atoms to vibrationally excited molecules, and similarly a slow change Δ_2 converts the vibrationally excited molecules into stable molecules. The process is defined $\Delta_i = |\Delta_i^{initial}| + |\dot{\Delta}_i|t$ and $|\dot{\Delta}_i| = \chi_i^2/10$ define slow.

Results are shown in Fig. 4.5. For the first step in (a) and (b), the same photoassociation parameters are used as Figs. 4.3(d) and (e), respectively. For the second step, the fixed parameters are $\Omega_3 = 10\Omega_4 = \delta_2 = 100\Gamma_0$, so that $\chi_2/\Gamma_2 = 1000$. The best yield is about 75% [Fig. 4.5(a)] but requires an impractically strong photoassociation laser, $I_1 = 14.2$ kW/cm^2, to compete against vibrational relaxation, even for low condensate density $\rho = 10^{12}$ cm^{-3}. Moderate coupling [Fig. 4.3(b)] requires less intensity, $I_1 = 1.42$ kW/cm^2, but the yield drops to about 65%. Atom-molecule conversion takes about 0.3 ms. Weak coupling, $\chi = 0.06\omega_\rho$ (not shown), requires only $I_1 = 150$ W/cm^2, but yields only 35% molecules.

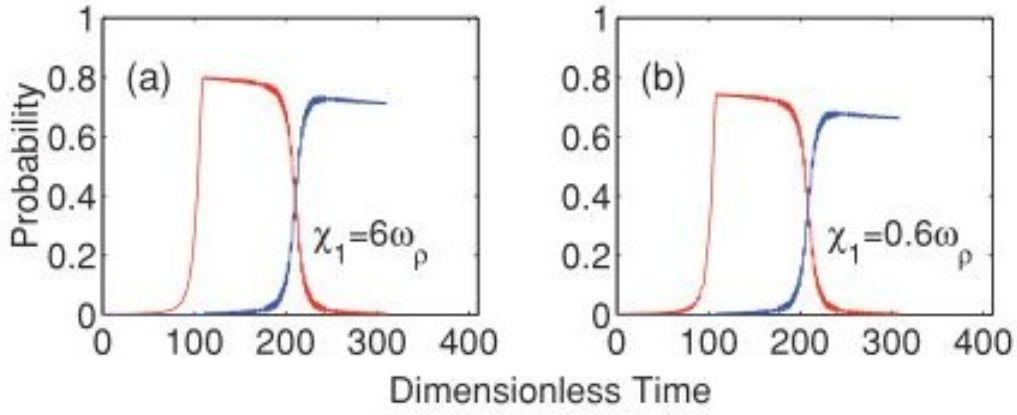

Figure 4.5: Four-laser scheme molecular probability vs. dimensionless time ($\tau_i = \chi_i t$) for two-step adiabatic following, at (a) strong and (b) moderate coupling. In the first step, atoms are turned into vibrationally excited molecules at $\tau \sim 100$. In the second step, molecules are converted from vibrationally excited to stable at $\tau \sim 200$.

4.3 Summary

Our results demonstrate that two-photon photoassociation via adiabatic following can be used to create a quantum degenerate gas of stable ^{7}Li-Na molecules relying on practical laser intensities. Changing the system from a positive detuning to a negative detuning changes the ground state from atoms to molecules, and molecules are thus created. Going in the other direction, the ground state changes from molecules to atoms; molecules are momentarily created, but then dissociate into noncondensate atom pairs. However, dissociation is only energetically accessible in the case where $\chi \gtrsim \omega_\rho$, and at weak coupling dissociated atom pairs are suppressed. As a result, weak coupling creates molecules going in both directions.

We find that low-intensity conversion remains efficient against reasonable increases in the strength of elastic s-wave collisions. Since the requisite laser intensity decreases for heavier particles, this method should be feasible for heavier species, as well as heteronuclear or homonuclear molecules, and most likely for other statistics as well. We also looked at a four-laser scheme, that creates stable molecules through

an intermediate, vibrationally-excited bound state. While transitions directly to the stable molecular state require the least photoassociation intensity, about 30 W/cm^2, transitions via the intermediate states require an impractically strong photoassociation laser, roughly 500 times stronger. Consequently, stable molecule creation using the two-laser scheme remains more favorable than the four-laser scheme.

CHAPTER 5

STABLE MOLECULES II: PULSED INTENSITY PHOTOASSOCIATION AND FESHBACH RESONANCE

In this chapter, we study yet another approach to creating quantum degenerate molecules, using pulsed laser photoassociation enhanced by strong magnetoassociation [76]. Previous research has shown that magnetoassociation can enhance one-photon photoassociation [66, 73, 78, 84, 128, 129], but whether or not this enhancement will carry over to two-photon photoassociation of stable molecules has yet to be confirmed. We focus on pulsed lasers, where one free-bound laser pulse creates electronically excited molecules and a bound-bound laser pulse couples the excited molecular state to a ground state [80]. This introduces the additional variable of pulse ordering, where the intuitive scheme has the free-bound laser occurring first, and the counterintuitive scheme has the bound-bound laser occurring first [80,130]. We model enhancement by coupling the atom state to a vibrationally excited molecular state via a strong magnetoassociation coupling. We find that strong magnetoassociation improves stable molecule formation using low-intensity photoassociation, independent of pulse ordering. This conversion efficiency decreases for stronger intra-atomic, molecular, and atom-molecule collisions, but increases for stronger inter-atomic collisions.

In the previous chapter, we studied the case of two-photon (Raman) photoassociation with a fixed intensity, varying frequency laser scheme. Here we investigate two-photon photoassociation with fixed frequency, pulsed intensity lasers to create stable quantum degenerate molecules. One laser pulse (pump pulse) couples the initial atomic ground state to an electronically excited molecular state, and a second laser pulse (dump pulse) couples the excited molecular state to a ground molecular state [80]. This method of pulsed lasers can be divided into two types, which is determined by the pulse order. In an intuitive pulse sequence, the pump laser

turns on first, and in a counter-intuitive pulse sequence (also known as stimulated rapid adiabatic passage or STIRAP), the dump laser turns on first [61, 131]. The counter-intuitive pulse has been shown to transfer population to the target state with near-unit efficiency [80, 130], however it requires high laser intensities [13, 127], which can be experimentally difficult to achieve. One possible route around this requirement is to enhance photoassociation using magnetoassociation.

Also referred to as a Feshbach resonance [12], magnetoassociation occurs when one atom in a colliding pair spin flips in the presence of a magnetic field tuned near a collision resonance, creating a bound molecule. While photoassociated molecules are electronically excited, the Feshbach molecules are vibrationally excited. There are then two loss channels, vibrational relaxation due to collisions and dissociation into a pair of atoms. Previous research has shown that strong magnetoassociation can enhance photoassociation [66, 73, 78, 79, 84, 128, 129], due to quantum interference between direct photoassociation and photoassociation via the Feshbach state [73, 79]. This enhancement should theoretically carry over to Raman photoassociation, and herein we examine whether such is the case. With the Feshbach state, the system consists of four levels: atoms, excited molecules, stable molecules, and Feshbach molecules. In the case of the counter-intuitive sequence, the near-unit efficiency should only work with an odd number of levels [132–135], due to the intermediate states being "dark," and should break down for an even number of levels [81, 82]. One possibility is that the dissociated atom pairs will act as an effective level, as it has on a separate occasion [68], enabling a fully effective counter-intuitive scheme. Even if the counterintuitive scheme is less than perfect, this still leaves open the question of whether it outperforms the intuitive scheme, and whether the additional level still provides enhancement over lasers alone, especially with the condition of low-intensity.

We model pulsed intensity Raman photoassociation with enhancement from

a Feshbach resonance, to create stable quantum degenerate molecules. The model includes relevant elastic collisions between particles, dissociative decay of the Feshbach molecules, as well as spontaneous and dissociative decay of the electronically excited photoassociation molecules. Collision-induced vibrational relaxation is ignored compared to the irreversible losses already included. We use two models, a second-quantized model that explicitly includes dissociated pairs and Feshbach molecules [68,83], and one that treats them as virtual [65,66,73,79,84,85,128,129,136]. Both the full and virtual models contrast with a previous model [61] where the Feshbach resonance was accounted for merely with a magnetically tunable collisional interaction.

We find that strong magnetoassociation can substantially improve weak-but not strong-Raman photoassociation, independent of pulse ordering. For larger pulse areas, the counter-intuitive sequence is more efficient for both weak and strong photoassociation, due to the excited state still being dark (numerically), even if the Feshbach molecular state is dim. In the mean-field model, vicarious photoassociation losses from the atomic state mean that peak enhancement occurs when the Feshbach detuning is large compared to the photoassociation line width. In the resonant-interaction model, peak enhancement occurs where the resonant inter-atomic interaction vanishes. Disagreement between the resonant-interaction and mean-field models on final conversion efficiencies and the nature of the dark state highlights the importance of explicitly including the Feshbach molecular state in modeling magnetoassociation enhanced photoassociation. Finally, whereas the peak conversion efficiency decreases for stronger intra-atomic, molecular, and atom-molecule collisions, we find that the peak conversion efficiency actually increases for stronger inter-atomic collisions. Systems with a combination of a strong Feshbach resonance and strong inter-atomic collisions will therefore be of greater experimental utility, compared to those with a strong

Feshbach resonance and weak inter-atomic collisions.

5.1 Model

In keeping with Ch. 4, we focus on a two-component condensate, motivated by the interest in the dipolar properties of the resulting heteronuclear molecules [26, 27, 30, 137–140], but our results also apply to homonuclear systems. However, any dipolar interaction is considered relevant only after the molecules are formed, and is not accounted for in the association process on the supposition that conversion from atoms to molecules is faster than any dipolar interaction. We also expect the results to apply to homonuclear systems.

In the few-level description illustrated in Fig. 5.1(a), we consider N_1 (N_2) atoms of species 1 (2) that have Bose condensed into the plane-wave state $|0_1\rangle$ ($|0_2\rangle$) with zero momentum $\hbar\vec{k} = 0$ which are represented in Fig. 5.1(a) as a single state $|0\rangle$ $= |0_1\rangle\ |0_2\rangle$. A photoassociation pump laser couples two atoms in the $|0\rangle$ state to an electronically excited molecule in the state $|1\rangle$, and a secondary dump laser couples the molecule in $|1\rangle$ to a molecule in the absolute ground state $|2\rangle$. Additionally, a magnetic field tuned nearby a Feshbach resonance couples the atom state in $|0\rangle$, to a vibrationally excited molecule in the state $|3\rangle$. In the full model of Fig. 5.1(a), the Feshbach and photoassociation molecules dissociate into noncondensate atom pairs

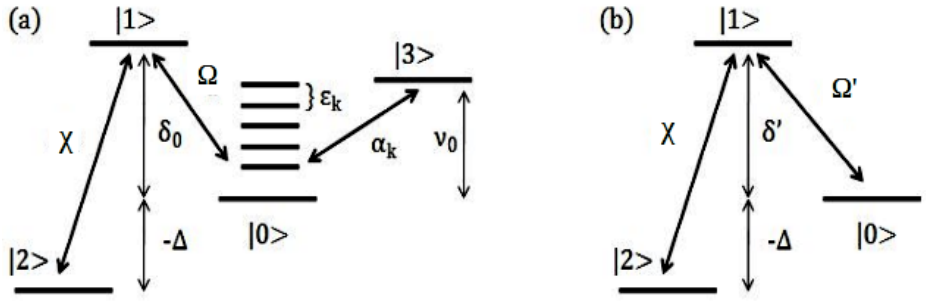

Figure 5.1: Feshbach-enhanced Raman photoassociation Models. (a) Full model, which explicitly includes dissociation states and Feshbach state. (b) Resonant-interaction model, after dissociation and Feshbach states have been adiabatically eliminated.

that occupy one of a discretized continuum of plane-wave states with momentum $\pm\hbar\vec{k} \neq 0$. In second-quantized notation, the Hamiltonian corresponding to Fig. 5.1(a) is

$$H = H_P + H_D + H_M + H_C, \tag{5.1}$$

where the contribution due to the photoassociation pump laser is

$$\frac{H_P}{\hbar} = \tilde{\delta}_0 b^\dagger b + \sum_{\vec{k}} \Omega_{\vec{k}} (b^\dagger a_{\vec{k},1} a_{-\vec{k},2} + a^\dagger_{-\vec{k},2} a^\dagger_{\vec{k},1} b), \tag{5.2}$$

the contribution due to the secondary dump laser is

$$\frac{H_D}{\hbar} = -\Delta g^\dagger g + \chi (g^\dagger b + b^\dagger g), \tag{5.3}$$

the contribution due to the magnetic field is

$$\frac{H_M}{\hbar} = \nu_0 c^\dagger c + \sum_{\vec{k}} \alpha_{\vec{k}} (c^\dagger a_{\vec{k},1} a_{-\vec{k},2} + a^\dagger_{-\vec{k},2} a^\dagger_{\vec{k},1} c), \tag{5.4}$$

and the contribution due to s-wave collisions in the condensates is

$$\frac{H_C}{\hbar} = \lambda_{00} c^\dagger c^\dagger c c + \lambda_{03} c^\dagger c g^\dagger g + \frac{1}{2} \sum_i a_i^\dagger a_i \left(\lambda_{0i} c^\dagger c + \lambda_{3i} g^\dagger g + \sum_j \lambda_{ij} a_j^\dagger a_j \right). \tag{5.5}$$

Here atoms in the ith condensate are represented by $a_i = a_{i,0}$, atoms with momentum $\hbar\vec{k}$ by $a_{i,\vec{k}}$, Feshbach molecular condensate by $c_0 = c$, photoassociation molecules by $b_0 = b$, and stable molecular condensate by $g_0 = g$. The detuning of the magnetic field from the Feshbach resonance is ν_0, spontaneous decay of the Feshbach molecules [141] is neglected, the one-photon laser detuning is $\delta_0 = \Re[\tilde{\delta}_0]$, the spontaneous decay rate for the photoassociation molecule is $\Gamma_s = 2\Im[\tilde{\delta}_0]$, and the two-photon detuning is Δ. The magnetic-field coupling between the atoms and the Feshbach molecules is $\alpha_{\vec{k}} = \alpha f_{M,\vec{k}}$, the pump-laser coupling between the atoms and the photoassociation molecules is $\Omega_{\vec{k}} = \Omega f_{P,\vec{k}}$, and the dump-laser coupling between the photoassociation and stable molecules is χ. The momentum dependence of the Feshbach and photoassociation couplings are contained in $f_{M,\vec{k}}$ and $f_{P,\vec{k}}$, respectively,

where $f_{\vec{k}=0} = 1$. Finally, the strength of collisions is determined by λ_{ij}, which is determined by the s-wave scattering length. Compared to the spontaneous decay rate, elastic collision involving primary photoassociation molecules are neglected, and we also neglect vibrational relaxation [126] of the photoassociation and Feshbach molecules.

5.1.1 Mean-Field Model

The mean-field model is derived from a c-number approximation to the Heisenberg equations, $i\hbar\dot{x} = [x, H]$, with x being the relevant operator, which generally works best for $N \gtrsim 100$ [69]. Dissociation of Feshbach and photoassociation molecules into noncondensate atoms pairs is accounted for with the operator $a_{\vec{k},1}a_{-\vec{k},2}$, and the corresponding c-number amplitude $A_{\vec{k}} = \langle a_{\vec{k},1}|a_{-\vec{k},2}\rangle$. The dissociation in momentum is converted into frequency according to $\sum_{\vec{k}} \to N/(4\pi^2\omega_\rho^{3/2})\int d\epsilon$, where $\hbar\epsilon = \hbar^2k^2/(2\mu)$ is the kinetic energy and $\omega_\rho = \hbar\rho^{2/3}/(2\mu)$ is the characteristic frequency for a dissociated pair, with ρ the total particle density and μ the reduced atomic mass.

This produces the equations

$$i\dot{a}_1 = \omega_1 a_1 - \frac{1}{2}\Omega a_2^* b - \frac{1}{2}\alpha a_2^* c, \tag{5.6a}$$

$$i\dot{a}_2 = \omega_2 a_2 - \frac{1}{2}\Omega a_1^* b - \frac{1}{2}\alpha a_1^* c, \tag{5.6b}$$

$$i\dot{b} = \tilde{\delta}_0 b - \frac{1}{2}\Omega a_1 a_2 - \frac{1}{2}\chi g - \frac{1}{2}\xi_P \int d\epsilon\sqrt{\epsilon} f_P(\epsilon) A(\epsilon), \tag{5.6c}$$

$$i\dot{c} = (\nu_0 + \omega_3)c - \frac{1}{2}\alpha a_1 a_2 - \frac{1}{2}\xi_M \int d\epsilon\sqrt{\epsilon} f_M(\epsilon) A(\epsilon), \tag{5.6d}$$

$$i\dot{g} = -(\Delta_0 - \omega_4)g - \frac{1}{2}\chi b, \tag{5.6e}$$

$$i\dot{A}(\epsilon) = \epsilon A(\epsilon) - \frac{1}{2}\Omega f_P(\epsilon) b - \frac{1}{2}\alpha f_M(\epsilon) c. \tag{5.6f}$$

Defining $\Lambda_{i\neq j} = \frac{1}{2}\rho\lambda_{ij}$ and $\Lambda_{i=j} = \rho\lambda_{ij}$, the shifts in the energy levels due to elastic

collisions are

$$\omega_1 = \Lambda_{11}|a_1|^2 + \Lambda_{12}|a_2|^2 + \Lambda_{01}|c|^2 + \Lambda_{13}|g|^2, \tag{5.7a}$$

$$\omega_2 = \Lambda_{12}|a_1|^2 + \Lambda_{22}|a_2|^2 + \Lambda_{02}|c|^2 + \Lambda_{23}|g|^2, \tag{5.7b}$$

$$\omega_3 = \Lambda_{01}|a_1|^2 + \Lambda_{02}|a_2|^2 + \Lambda_{00}|c|^2 + \Lambda_{03}|g|^2, \tag{5.7c}$$

$$\omega_4 = \Lambda_{13}|a_1|^2 + \Lambda_{23}|a_2|^2 + \Lambda_{03}|c|^2 + \Lambda_{33}|g|^2. \tag{5.7d}$$

Finally, the photodissociation and magnetoassociation couplings are $\xi_P = \Omega/4\pi^2\omega_\rho^{3/2}$ and $\xi_M = \alpha/4\pi^2\omega_\rho^{3/2}$, respectively.

5.1.2 Resonant-Interaction Model

The resonant-interaction model is derived by first treating the dissociated pair amplitude adiabatically ($\dot{A} = 0$), which is equivalent to the limit of weakly bound molecules [73,79], and leads to the effective four-level system [Fig. 5.1(b)] with mean-field equations of motion

$$i\dot{a}_1 = \omega_1 a_1 - \frac{1}{2}\Omega a_2^* b - \frac{1}{2}\alpha a_2^* c, \tag{5.8a}$$

$$i\dot{a}_2 = \omega_2 a_2 - \frac{1}{2}\Omega a_1^* b - \frac{1}{2}\alpha a_1^* c, \tag{5.8b}$$

$$i\dot{b} = \tilde{\delta} b - \frac{1}{2}\Omega a_1 a_2 - \frac{1}{2}\chi g - \frac{1}{2}\kappa c, \tag{5.8c}$$

$$i\dot{c} = (\tilde{\nu}_0 + \omega_3)c - \frac{1}{2}\alpha a_1 a_2 - \frac{1}{2}\kappa b, \tag{5.8d}$$

$$i\dot{g} = -(\Delta_0 - \omega_4)g - \frac{1}{2}\chi b, \tag{5.8e}$$

The virtual continuum leads to an effective coupling between the Feshbach and photoassociation molecules [73, 79] of strength

$$\kappa = \frac{1}{8\pi}\frac{\alpha\Omega}{\omega_\rho^{3/2}}\Re\left[\lim_{\epsilon_0\to 0}\int d\epsilon\sqrt{\epsilon}\frac{f_M(\epsilon)f_P(\epsilon)}{\varepsilon - \epsilon_0}\right]. \tag{5.9}$$

Additionally, there are real and imaginary shifts [73] for each molecular detuning: $\tilde{\nu} = \nu_0 - \sigma_M - i\gamma_M/2$ and $\tilde{\delta} = \tilde{\delta}_0 - \sigma_P - i\gamma_P/2$, where $\sigma_{M(P)} = \Re[\Sigma_{M(P)}]$ and

$\gamma_{M(P)} = \Im[\Sigma_{M(P)}]$ with

$$\Sigma_M = \frac{1}{8}\alpha\xi_M \left[\lim_{\epsilon_0\to 0}\int d\epsilon\sqrt{\epsilon}\frac{f_M^2(\epsilon)}{\varepsilon-\epsilon_0}\right], \tag{5.10a}$$

$$\Sigma_P = \frac{1}{8}\Omega\xi_P \left[\lim_{\epsilon_0\to 0}\int d\epsilon\sqrt{\epsilon}\frac{f_P^2(\epsilon)}{\varepsilon-\epsilon_0}\right]. \tag{5.10b}$$

The real shift is the result of coupling a bound state to a continuum [48, 108–111], and the imaginary shift is the dissociation rate. In this case, σ_M is static, while the photoassociation σ_P shift is transient, and both are treated as implicit in the detuning rather than explicitly.

Next, we arrive at the resonant-interaction model by treating the Feshbach amplitude adiabatically ($\dot{c} = 0$), which is the limit of large detuning of the magnetic field from the Feshbach resonance, and leads to an effective three-level system,

$$i\dot{a}_1 = \omega_1' a_1 - \frac{1}{2}\Omega' a_2^* b, \tag{5.11a}$$

$$i\dot{a}_2 = \omega_2' a_2 - \frac{1}{2}\Omega' a_1^* b, \tag{5.11b}$$

$$i\dot{b} = \tilde{\delta}' b - \frac{1}{2}\Omega' a_1 a_2 - \frac{1}{2}\chi g, \tag{5.11c}$$

$$i\dot{g} = -(\Delta_0 - \omega_4)g - \frac{1}{2}\chi b, \tag{5.11d}$$

As detailed previously [65, 66, 73, 79, 84, 85, 128, 129, 136], in the resonant-interaction model the Feshbach resonance effectively modifies the photoassociation interaction $\Omega' = \Omega - \alpha\kappa/\omega$, and the detuning $\tilde{\delta}' = \delta' - i\Gamma'/2$, with an effective detuning $\delta' = \delta - \kappa^2/\omega$ and an effective decay rate $\Gamma' = \Gamma + (\kappa^2/\omega^2)\gamma_M$, where $\Gamma = \Gamma_s + \gamma_P$. Finally, we find the usual resonant collisional interaction, where $\omega_1' = \Lambda_{11}|a_1|^2 + \Lambda_{12}'|a_2|^2 + \Lambda_{01}|c|^2 + \Lambda_{13}|g|^2$, $\omega_2' = \Lambda_{12}'|a_1|^2 + \Lambda_{22}|a_2|^2 + \Lambda_{02}|c|^2 + \Lambda_{23}|g|^2$, and $\Lambda_{12}' = \Lambda_{12} - \alpha^2/2\omega$. In one-photon transitions [73, 79], collisions—resonant or otherwise—are neglected compared to the spontaneous decay rate, but here the time scale for conversion is long enough, especially in the counterintuitive scheme, that collisions become relevant.

Depending on the sign of the Feshbach detuning, the modified photoassoci-

ation coupling can be greater than the unmodified coupling, zero, or less than the unmodified coupling. Similarly, the real part of the resonant contribution to the photoassociation detuning, κ^2/ω, can produce a red shift, no shift, or a blue shift, as opposed to the ambient shift, σ_P, which is strictly to the red [48,108–111]. Moreover, the resonant contribution to the decay rate, $(\kappa^2/\omega^2)\gamma_M$, leads to decay that depends on magnetic field and diverges near the Feshbach resonance.

To model the pulsed intensity, we use Gaussian shaped pump and dump couplings. The pulses are

$$\Omega(t) = \Omega_0 \exp[-\frac{(t-T_p)^2}{2\tau_p^2}], \tag{5.12a}$$

$$\chi(t) = \chi_0 \exp[-\frac{(t-T_d)^2}{2\tau_d^2}]. \tag{5.12b}$$

where Ω_0 (χ_0) is the pump (dump) pulse amplitude, T_p (T_d) is the time at which the peak occurs. The pulse width is τ_p (τ_d), and determines the timescale for the pulse. The timing of the pulses determines the amount that the pulses overlap as well as the timing sequence, as shown in Fig. 5.2. The intuitive pulse sequence is pump-dump,

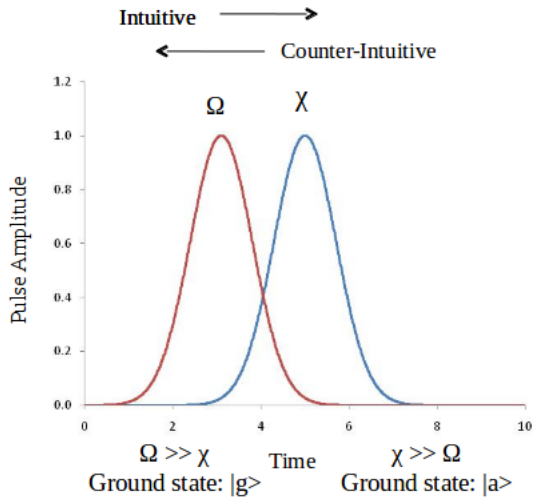

Figure 5.2: Laser pulse timing sequence. In the intuitive sequence, Ω precedes χ, and the ground state evolves from molecules to atoms. Conversely, in the counter-intuitive sequence, χ precedes Ω, and the ground state evolves from atoms to molecules.

whereas the counter-intuitive sequence is dump-pump.

The counter-intuitive case gets its name from the intuition that population transfer to the ground state is predicated on the pump pulse coming first, since transition must somehow include the excited state. One way to properly understand this is to treat the scheme similarly to the adiabatic following scheme from Ch. 4, assuming the adiabatic condition applies [131]. Treating the case where $\Omega \gg \chi$, atoms are energetically favored, so that molecules can be considered to be the ground state. In the opposite case $\chi \gg \Omega$, molecules are energetically favored, making atoms the ground state. In the case of the pump-dump scheme, the system then begins with molecules as the ground state and then ends with atoms as the ground state. In the dump-pump scheme, the system begins with atoms as the ground state, and ends with molecules as the ground state. The issue arises in the case of low laser intensity, in which case the adiabatic condition requires longer pulses, which then means the photoassociation timescales approach those of collisions.

5.2 Parameters and Results

Considering the parameter values, the strength of the free-bound association couplings are measured relative to the characteristic frequency ω_ρ [68, 69] and, for consistency, so are the collisional couplings. Hence, we consider a strong magnetoassociation coupling $\alpha \gg \omega_\rho$, as well as both strong ($\Omega_0 \gg \omega_\rho$) and weak ($\Omega_0 \lesssim \omega_\rho$) photoassociation. Finally, collisions are pre-mitigated to a certain extent with low density [61] $\rho = 10^{12}$ cm^{-3}, and we assign elastic collisional couplings that range from weak to moderate.

In particular, the Feshbach coupling is $\alpha = 134.8$, the weak (strong) photoassociation pump coupling is $\Omega_0 = 15.4(154)$, and the spontaneous decay rate for $\Omega_0 = 154$ is $\Gamma_s = 41\Omega_0$. Here strong photoassociation corresponds to a laser set at the saturation intensity and, since $\Omega \propto \sqrt{I}$, the weak coupling corresponds to an inten-

sity two orders of magnitude below the saturation intensity [14, 15, 70, 96, 98]. In the counterintuitive scheme, the dump coupling is $\chi_0 = 50\Omega_0$, but the intuitive scheme is more efficient for $\chi_0 = \Omega_0$. The respective coupling to the dissociation continuum is then determined by the Lorentzian $f_i = 1/(1+\varepsilon^2/\beta_i^2)$, which is in turn determined by the molecular size $\beta_i = \hbar/mL_i^2$. For magnetoassociation we choose a point particle, $L_M = \rho^{-1/3}$, and for photoassociation we choose a typical size, $L_P = 130a_0$, where a_0 is the Bohr radius. For the collisional couplings, we choose values for λ_{ij} such that $\Lambda_{00} = \Lambda_{30} = 0.8$, $\Lambda_{11} = 5.1\times10^{-3}$, $\Lambda_{22} = 2.1\times10^{-2}$, $\Lambda_{12} = 4\times10^{-2}$, $\Lambda_{33} = 8.1\times10^{-3}$, $\Lambda_{13} = 4.3\times10^{-2}$, and $\Lambda_{23} = 1.9\times10^{-2}$. Finally, in the tunable collision model, the magneto-dissociation rate is $\gamma_M/\Gamma_s = 7.4\times10^{-2}$, the photodissociation rate for strong (weak) coupling is $\gamma_p/\Gamma_s = 1$ (1/100), and the peak cross-molecular coupling is $\kappa_0 = 3.9\times10^3$ (3.9×10^4) for weak (strong) photoassociation.

To give the counterintuitive scheme the best chance for success, i.e., slow enough to be considered adiabatic but fast enough to outrun ambient collisions, we set the pulse width according to $\Omega_0\tau = 5\times10^3$, where we set the pulse widths equal to each other, $\tau_p = \tau_d = \tau$. Also, to ease the numerical overhead we only optimize the one-photon detuning δ, which is consistent with the expected dispersive-like behavior [65, 73, 79]. The counter-intuitive pulse delay is fixed to $D = T_1 - T_2 = -2\tau$, and we also fix the two-photon detuning to resonance ($\Delta = 0$) in the weak case and Stark-shifted resonance ($\Delta = \Omega_0^2/2\delta$) in the strong case. For the intuitive scheme, coincident pulses ($D = 0$) are generally optimal for all magnetic fields, both the pulse width and one-photon detuning are optimized at each magnetic field, but the two-photon detuning is again fixed to resonance in the weak case and Stark-shifted resonance in the strong case.

5.2.1 Feshbach Enhancement

Results are presented in Fig. 5.3 for [(a)-(d)] weak photoassociation and [(e)-(h)] strong photoassociation. Below resonance, The node arises from destructive interference between direct photoassociation and indirect photoassociation occurring via the Feshbach molecular state [73, 79]. On resonance, a second node appears, and in the full model this node is due to the absence of an atom-molecule dark state that includes both excited molecules, while in the effective model it is due to divergence of the magnetically tunable decay rate. Regarding the magnitude of peak enhancement, for weak coupling the magnetic field enhances both schemes by about a factor of five, and the counterintuitive scheme outperforms the intuitive scheme by about 10% in the full model, and the two are roughly tied in the resonant-interaction model. Strong photoassociation is enhanced very little, to about about 80%, regardless of pulse order. The agreement with the full model is reasonable given the simplicity of the effective model. It is worth noting that a model where the primary photoassociation molecule is virtual instead of the Feshbach molecule improves the agreement between the two models near magnetic resonance, but worsens the off-resonant disagreement.

Focusing on weak photoassociation, improvements to the counterintuitive scheme can be made by increasing the pulse area from $\Omega_0\tau = 5\times10^5$ to 2.2×10^5 (6×10^5) in the resonant-interaction (mean-field) model, whereby the maximally enhanced counterintuitive efficiency improves from 30% to nearly 50% (76%). In the resonant-interaction model, further improvements can also be made by setting the pulse area according to Ω' instead of Ω, but this would require a change in the dump coupling to $\chi = 50\Omega'$, in order to satisfy the conditions for adiabatic following (specifically, $\chi \gg \Omega$ for $t \to -\infty$ and $\Omega \gg \chi$ for $t \to \infty$), and therefore would require an impractical amount of dump laser intensity as Ω' diverges on resonance. More importantly, this improvement is misleading since a larger peak dump pulse does not improve conversion in

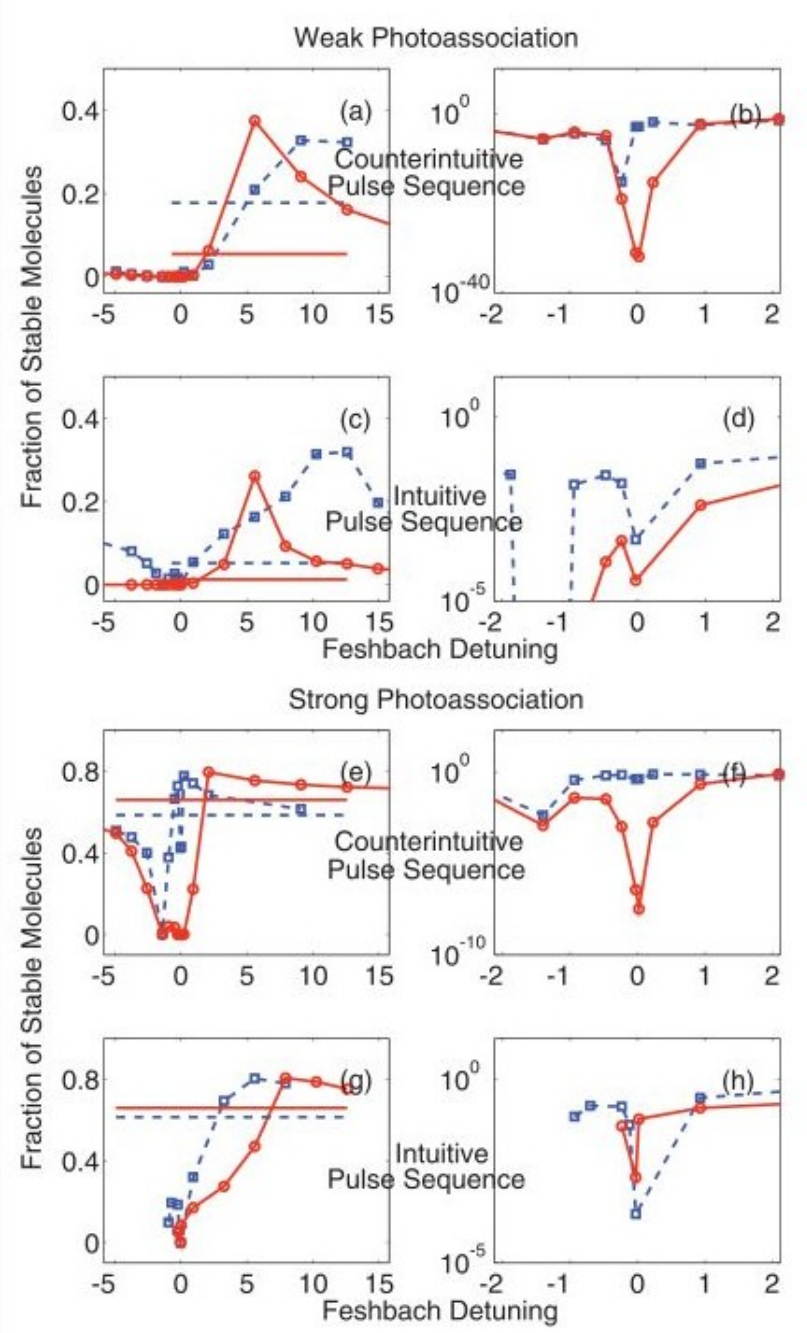

Figure 5.3: Feshbach-stimulated Raman photoassociation of a two-component Bose-Einstein Condensate for weak photoassociation [(a)-(d)] and strong photoassociation [(e)-(h)]. The solid lines and solid with circle markers represent results for the mean-field model with zero magnetic field and varying magnetic field, respectively, while the dashed and dashed with squares represent the magnetically-tunable model. The Feshbach detuning ω is in units Γ_s.

the full model, which we attribute to the absence of a dark state that includes both photoassociation and Feshbach molecules.

The dip near resonance and the off-resonant peak together indicate that enhancement from magnetoassociation does not account for the results alone, since Feshbach enhancement peaks near magnetic resonance [65, 73, 79]. In the full model, cross-coupling between the photoassociation and Feshbach molecules arises due to the shared dissociation continuum [61], which effectively enhances the weak photoassociation coupling to be comparable to the Feshbach coupling, but it also enhances the Feshbach losses to be comparable to the photoassociation losses. In other words, the Feshbach molecular state decays vicariously through the photoassociation state, and peak enhancement therefore occurs where the Feshbach detuning is large compared to the spontaneous decay rate of the photoassociation state, roughly $\omega/\Gamma_s \approx 5$ in Fig. 5.3.

Although a completely dark state is absent, it so happens that the photoassociation state is dark and the Feshbach state is dim. In weak photoassociation, collisions disrupt the dark state and conversion is independent of pulse sequence for short pulses, and longer pulses help the counterintuitive scheme until the time scale for collisions is reached. In strong photoassociation, collisions play a lesser role. For a counterintuitive pulse sequence, the dark photoassociation state then allows efficient conversion closer to the Feshbach resonance, and the enhancement peak shifts to the red. For an intuitive pulse sequence where the dark state is moot, stronger laser coupling requires larger Feshbach detuning to combat vicarious losses, and the peak shifts to the blue. As with lasers alone, the peak efficiency decreases with increasing strength of intra-atomic, molecular, or atom-molecule collisions.

In terms of the effective model, peak improvement in the weak case occurs roughly where the resonant collisional interaction vanishes $\Lambda'_{12} = 0$, or $\omega/\Gamma_s =$

$\alpha^2/(4\Lambda_{12}\Gamma_s) \approx 9$, regardless of pulse sequence. For strong photoassociation, collisions again play a lesser role, and the counterintuitive scheme is more efficient closer to resonance, even closer than in the mean-field model due to the dim state in the effective three-level model. For the intuitive pulse sequence, the difference is made up-perhaps coincidentally-by the peak laser contribution to the resonant collisional interaction, $-\Omega_0^2/(4\delta)$. For weak or strong photoassociation, with tunable collisions nulled, the conversion efficiency is determined by the non-tunable collisional interactions. That peak improvement occurs where the magnetically tunable collisional interaction vanishes, and that the magnitude of peak improvement is determined by non-tunable collisions, is in line with previous work on Raman photoassociation of an interacting Bose condensate [60, 61] combined with a far-detuned Feshbach resonance [61].

The role of Feshbach enhancement can be understood further by considering the magnetically tunable parameters in the effective model [Fig. 5.4], where panel (a) corresponds to the parameters in Fig. 5.3. The resonant decay rate drops relatively quickly to its ambient value, and the photoassociation coupling follows shortly thereafter, but it is not until the resonant collisional interaction reaches a reasonable value ($\omega/\Gamma_s \lesssim 9$) that any improvement kicks in. At peak enhancement, the photoassociation coupling, weak or strong, is enhanced to $\Omega'/\Omega = 1.2$, which amounts to an effective increase in intensity of a factor of about 1.4. Part of the reason for the lackluster improvement in strong photoassociation is due to its already being saturated [14, 15, 70, 96, 98], so any increase in coupling is moot.

What is unexpected is that while an increase in the strength of non-tunable collisions (intra-atom, molecule, or atom-molecule) will decrease the conversion efficiency [60, 61], an increase in the ambient value of the tunable inter-atomic collisional interaction, Λ_{12}, will actually increase the efficiency of stable molecule production.

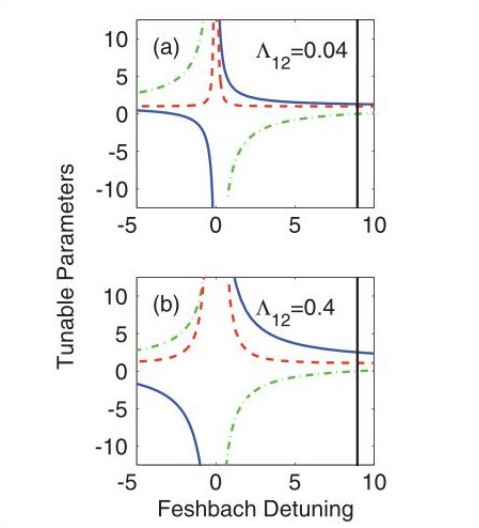

Figure 5.4: Magnetically tunable parameters vs. Feshbach detuning for weak photoassociation. The solid line is the photoassociation coupling (Ω_R/Ω). the dashed line is the tunable PA decay rate (Γ_R/Γ), and the dot-dashed line is the tunable collisions (Λ_T/Λ_{12}). The vertical line denotes $\Lambda_R = 0$, the dimensionless Feshbach detuning is defined ω/Γ_s, and the parameters in (a) are the same as in Fig. 5.3.

In particular, since the magnetoassociation coupling [12, 36, 142, 143] $\alpha \propto \sqrt{\Lambda_{12}}$, the Feshbach-detuning location of $\Lambda'_{12} = 0$, i.e., $\omega_z = \alpha^2/4\Lambda_{12}$, is independent of Λ_{12}. At the magnetic-field location of peak enhancement, ω_z, the resonant contribution to the photoassociation coupling is $\alpha\kappa/(2\omega_z) \propto \Lambda_{12}$, and stronger inter-atomic collisions therefore lead to stronger Feshbach enhancement at $\omega = \omega_w$, as illustrated in Fig. 5.4(b) for weak photoassociation and $\Lambda_{12} \to 10\Lambda_{12}$. For the counterintuitive scheme at a pulse area of $\Omega_0\tau = 5 \times 10^3$, in the resonant-interaction model a factor of two (ten) increase in Λ_{12} enhances conversion from 30% to 37% (60%), and in the mean-field model the former (latter) increase in Λ_{12} enhances conversion from 30% to 42% (67%).

5.2.2 Analytical Results

Deriving a two-level system from Eqs. 5.11 in the limit of large Feshbach-shifted detuning ($\nu \gg \Gamma_s$), and then deriving a rate equation for the atom losses [73, 79], we obtain the rate constant for Feshbach-enhanced Raman photoassociation for cw

lasers

$$\rho K = \frac{1}{4}\frac{\chi_2^2\Gamma_2}{\sigma_{mf})_R^2 + \Gamma_2^2/4}, \tag{5.13}$$

where the tunable two-photon coupling is $2\chi_2 = \Omega'\chi/\delta'$, the tunable two-photon decay rate is $4\Gamma_2 = (\chi/\delta')^2\Gamma'$, and the tunable mean-field shift is approximated to the static value $\sigma_{mf})_R = \sigma_{mf} + 2\Lambda'_{12}$ with the nonresonant mean field shift $\sigma_{mf} = \Lambda_{11} + \Lambda_{22} - (\Lambda_{13} + \Lambda_{23} + \Lambda_{33})$.

The results shown in Fig. 5.5 for weak photoassociation with $\delta' = 10\Gamma_s$ are broadly consistent with Fig. 5.3. In particular, the dip below the Feshbach resonance corresponds to $\Omega' = 0$. The peak in atom losses at the Feshbach resonance corresponds to a peak in two-photon losses, which corresponds to the decreased molecule formation near Feshbach resonance in Fig. 5.3. The peak far above the Feshbach resonance arises from $\Lambda'_{12} = \sigma_{mf}/2$, which corresponds to the numerical peak for $\Lambda'_{12} = 0$. We attribute the difference to the static mean-field shift approximation that neglects transient populations, which also leads to a peak location that is not independent

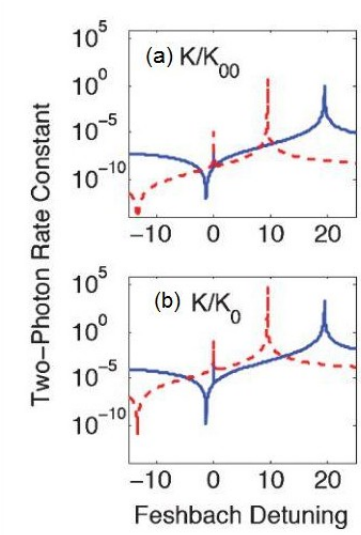

Figure 5.5: Rate Constant for weak Feshbach-enhanced Raman photoassociation compared to the unenhanced rate constant for (a) a noninteracting condensate (K_{00} and (b) an interacting K_0 condensate. The solid (dashed) lines correspond to $\Lambda_{12} = 0.04(0.4)$. Detuning is defined ω/Γ_s.

of Λ_{12}. Nevertheless, for $\Lambda_{12} = 0.04$ the enhanced two-photon rate constant peaks at roughly the value for a noninteracting gas, $K_{00} = \chi_{20}^2/\Gamma_{20}$, and for $\Lambda_{12} = 0.4$ it increases to $K \sim 5K_{00}$. Moreover, compared to the $\alpha = 0$ result for an interacting condensate, $4K_0 = \chi_{20}^2\Gamma_{20}/[\sigma_{mf})_0 + \Gamma_{20}^2/4]$, the Feshbach resonance enhances the rate two-photon constant by roughly three orders of magnitude for $\Lambda_{12} = 0.04$, which increases to well over four orders of magnitude for $\Lambda_{12} = 0.4$. Note that $2\chi_{20} = \Omega\chi/\delta$, $4\Gamma_{20} = (\chi/\delta)^2(\Gamma_s + \gamma_{PA})$, and $\sigma_{mf})_0 = \sigma_{mf} + 2\Lambda_{12}$.

Before closing, we emphasize that the two-photon detuning has not been optimized in our numerical experiments, and that the laser detunings in general have not been chirped [77], both of which could lead to further improvements. Also, while comparisons between thermal and condensate systems should be taken with a grain of salt, the results for Feshbach enhancement in a thermal gas [144] indicate reduced efficiency upon averaging over density, and improved efficiency for narrower Feshbach resonance. Off hand, in association of an interacting condensate the atom-molecule coupling $\propto \sqrt{\rho}$ and the collisional coupling $\propto \rho$. Collisions therefore play the biggest role at the center of the trap, and inhomogeneity should have less of an effect on final conversion efficiencies in a local density approximation. Nevertheless, we look forward to a full investigation-including an explicit trapping potential of condensate inhomogeneity for both wide and narrow Feshbach resonances.

5.3 Summary

In short, we find that strong magnetoassociation can substantially improve weak Raman photoassociation, independent of pulse ordering. This enhancement does not occur in strong photoassociation, due to an already-saturated transition from atoms to molecules. The independence of pulse ordering is due to an unoptimized pulse widths for the counter-intuitive pulse order. For larger pulse areas, the counter-intuitive sequence is more efficient, since the photoassociation molecular state is still

dark (numerically), even if the Feshbach molecular state is dim.

In the mean-field model, vicarious photoassociation losses from the atomic state mean that peak enhancement occurs when the Feshbach detuning is large compared to the photoassociation line width. In the resonant-interaction model, peak enhancement occurs where the resonant inter-atomic interaction vanishes. Also, disagreement between the resonant-interaction and mean-field models on final conversion efficiencies and the nature of the dark state highlights the importance of explicitly including the Feshbach molecular state in modeling magnetoassociation.

Finally, whereas the peak conversion efficiency decreases for stronger intra-atomic, molecular, and atom-molecule collisions, we find that the peak conversion efficiency actually increases for stronger inter-atomic collisions. Systems with a combination of a strong Feshbach resonance and strong inter-atomic collisions will therefore be of greater experimental utility, compared to those with a strong Feshbach resonance and weak inter-atomic collisions. While this scheme shows that stable molecules can be created using weak photoassociation, it still depends on a strong associative process, in this case magnetoassociation is strong. In the next chapter, we therefore investigate the possibility of creating stable molecules using both weak photoassociation and weak magnetoassociation.

CHAPTER 6

STABLE MOLECULES III: LASER-ASSISTED WEAK PHOTOASSOCIATION AND WEAK MAGNETOASSOCIATION

In this chapter, we study another route to stable quantum degenerate molecules. We propose a scheme of weak photoassociation and weak magnetoassociation, enhanced by a bound-bound laser coupled to the Feshbach state. Previous studies have shown that the additional laser enhances strong magnetoassociation [86,87], but whether or not this enhancement holds for weak magnetoassociation as well has yet to be confirmed. We find that adding the bound-bound laser in the case of weak magnetoassociation and weak photoassociation improves the efficiency of ground state molecule formation. The most improvement in efficiency is observed for the strongest collision strength tested, where the laser-assisted system is twice as effective as Feshbach-enhanced photoassociation. This improvement opens the door to stable molecules for weak magnetoassociation.

In Ch. 4, we found that weak Raman photoassociation is a viable method for creating quantum degenerate molecules, and in Ch. 5, that strong magnetoassociation provides an additional boost. However, desired systems may not possess the wide Feshbach resonance required for strong magnetoassociation [12]. On the other hand, a laser provides a cheaper, more flexible option. Therefore, we investigate the addition of a bound-bound laser to assist Feshbach-enhanced Raman photoassociation. The additional laser couples the Feshbach-excited molecular state to a higher-lying vibrational bound state. Studies have shown that coupling the Feshbach state to an optical bound-bound transition can enhance magnetoassociation [86, 87], simulating a wider Feshbach resonance.

The question then is whether the assisting laser would lead to more efficient ground state molecules using weak photoassociation and weak magnetoassociation,

since the laser transition also leads to more spontaneous decay. The laser-assisted system could also lead to further experimental applications, since the excited state leaks at a much faster rate than Feshbach molecules. The expected advantage of this approach is that even though it requires an additional laser, it will still provide the strong coupling needed to associate atoms into molecules, and do so for reasonable laser intensity. Even if the proposed scheme is less than perfect, the question of enhancement over weak Feshbach resonance still remains. Using a model based on ^{7}Li with a strong collision strength, we compare stable molecule formation using weak photoassociation alone, weak magnetoassociation enhancement, and the laser-assisted scheme. To model the system under more restrictive conditions, we also consider stronger s-wave elastic collisions.

We find that adding a bound-bound laser in the case of weak magnetoassociation and weak photoassociation can improve the efficiency of ground state molecule conversion. The most improvement in efficiency is observed for the strongest collision strength tested, where the laser-assisted system is twice as effective as weak Feshbach-enhanced photoassociation. Consequently, this study is proof of principle that the enhanced system offers more flexibility to optimize the experimental setup based on whatever resource is more readily available, while still remaining highly efficient vs. realistic limiting factors.

6.1 Model

We focus on a homonuclear system where N atoms have Bose condensed into the $|0\rangle$ plane-wave state with zero momentum $\hbar\vec{k} = 0$. In the few-level description illustrated in Fig. 6.1(a), a photoassociation (pump) laser couples two atoms in the $|0\rangle$ state to an electronically excited molecule in the state $|1\rangle$, and a secondary (dump) laser couples the molecule in $|1\rangle$ to a molecule in the absolute ground state $|2\rangle$. A magnetic field tuned nearby a Feshbach resonance also couples the atom state in

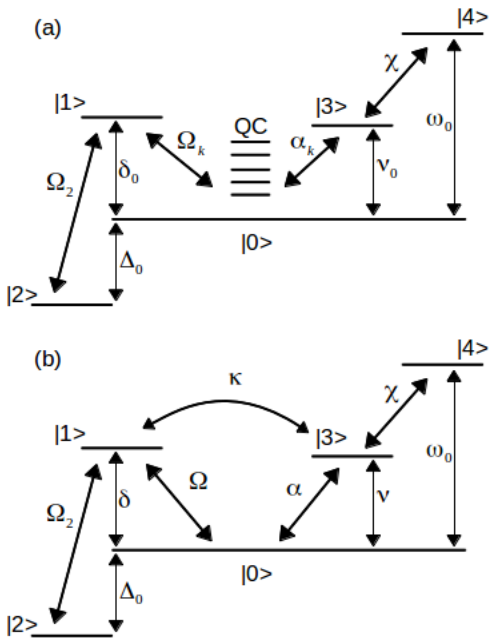

Figure 6.1: Basic model for laser-assisted Feshbach-enhanced photoassociation. (a) Mean-field model with quasicontinuum of dissociation states. (b) Model with effective cross-coupling.

$|0\rangle$ to a vibrationally excited molecule in the state $|3\rangle$, and the additional assisting bound-bound laser couples a molecule in the $|3\rangle$ state to a triplet vibrationally-excited molecular state $|4\rangle$.

In the full model of Fig. 6.1(a), the Feshbach and photoassociation molecules dissociate into noncondensate atom pairs that occupy one of a quasicontinuum of states, say, plane-wave states of momentum $\pm\hbar\vec{k} \neq 0$. In second-quantized notation, the Hamiltonian corresponding to Fig. 6.1(a) is

$$H = H_P + H_D + H_M + H_B + H_C, \tag{6.1}$$

where the contribution due to the photoassociation (pump) laser is

$$\frac{H_P}{\hbar} = \tilde{\delta}_0 b^\dagger b - \frac{1}{2}\sum_{\vec{k}} \Omega_{1\vec{k}}(b^\dagger a_{\vec{k}} a_{-\vec{k}} + a^\dagger_{-\vec{k}} a^\dagger_{\vec{k}} b), \tag{6.2}$$

the contribution due to the secondary (dump) laser is

$$\frac{H_D}{\hbar} = -\Delta_0 g^\dagger g - \frac{1}{2}\Omega_2(g^\dagger b + b^\dagger g), \tag{6.3}$$

the contribution due to the magnetic field is

$$\frac{H_M}{\hbar} = \nu_0 c^\dagger c - \frac{1}{2}\sum_{\vec{k}} \alpha_{\vec{k}}(c^\dagger a_{\vec{k}} a_{-\vec{k}} + a^\dagger_{-\vec{k}} a^\dagger_{\vec{k}} c), \tag{6.4}$$

the contribution due to the assisting bound-bound laser is

$$\frac{H_B}{\hbar} = \tilde{\omega}_0 d^\dagger d + \chi(d^\dagger c + c^\dagger d), \tag{6.5}$$

and the contribution due to s-wave collisions in the condensates is

$$\frac{H_C}{\hbar} = \frac{1}{2}\sum_i x_i^\dagger x_i \sum_j \lambda_{ij} x_j^\dagger x_j. \tag{6.6}$$

Here atoms in the ith condensate are represented by $a_i = a_{i,0}$, atoms with momentum $\hbar\vec{k}$ by $a_{i,\vec{k}}$, Feshbach molecular condensate by $c_0 = c$, photoassociation molecules by $b_0 = b$, the additional assisting molecules by $d_0 = d$, and stable molecular condensate by $g_0 = g$. The detuning of the magnetic field from the Feshbach resonance is ν_0, spontaneous decay of the Feshbach molecules is neglected, the one-photon laser detuning is $\delta_0 = \Re[\tilde{\delta}_0]$, the spontaneous decay rate for the photoassociation molecule is $\Gamma_1 = 2\Im[\tilde{\delta}_0]$, the assisting laser detuning is $\omega_0 = \Re[\tilde{\omega}_0]$, while the spontaneous decay rate for the assisting molecule is $\Gamma_2 = 2\Im[\tilde{\omega}_0]$, and the two-photon detuning is Δ_0. The magnetic-field coupling between the atoms and the Feshbach molecules is $\alpha_{\vec{k}} = \alpha f_{M,\vec{k}}$, the pump-laser coupling between the atoms and the photoassociation molecules is $\Omega_{p,\vec{k}} = \Omega_p f_{P,\vec{k}}$, and the dump-laser coupling between the photoassociation and stable molecules is Ω_d, and the assisting laser coupling between the Feshbach and bound-bound molecular states is χ. The momentum dependence of the Feshbach and photoassociation couplings are contained in $f_{M,\vec{k}}$ and $f_{P,\vec{k}}$, respectively, where $f_{\vec{k}=0} = 1$. Finally, the strength of collisions is determined by λ_{ij}, which is determined by the

s-wave scattering length. Since we are primarily interested in the magnetoassociation and photoassociation production of molecules, we neglect vibrational relaxation of the photoassociation and Feshbach molecules [126] and three-body losses which occur at much slower rates, as well as dipole interactions which are only considered relevant after molecules have formed.

The mean-field model is derived from a c-number approximation to the Heisenberg equations, $i\hbar\dot{x} = [x, H]$, with x being the relevant operator, which generally works best for $N \gtrsim 100$ [69]. A quasicontinuum of molecules that dissociate from Feshbach and photoassociation molecules back into noncondensate atom pairs is accounted for with the operator $a_{\vec{k},1}a_{-\vec{k},2}$, and the corresponding c-number amplitude $A_{\vec{k}} = \langle a_{\vec{k},1}a_{-\vec{k},2}\rangle$. Lastly, the quasicontinuum in momentum representation is converted into a continuum in frequency according to $\sum_{\vec{k}} \to N/(4\pi^2\omega_\rho^{3/2})\int d\epsilon$, where $\hbar\epsilon = \hbar^2k^2/(2\mu)$ is the kinetic energy and $\omega_\rho = \hbar\rho^{2/3}/(2\mu)$ is the characteristic frequency for a dissociated pair, with ρ equals the total particle density and μ the reduced atomic mass. The resulting equations of motion are given by

$$i\dot{a} = \Lambda_a a - \Omega_1 a^* b - \alpha a^* c, \tag{6.7a}$$

$$i\dot{b} = (\tilde{\delta}_0 + \Lambda_b)b - \frac{1}{2}\Omega_1 a^2 - \frac{1}{2}\Omega_2 g - \xi_P \int d\epsilon\sqrt{\epsilon} f_P(\epsilon)A(\epsilon), \tag{6.7b}$$

$$i\dot{c} = (\nu_0 + \Lambda_c)c - \frac{1}{2}\alpha a^2 - \frac{1}{2}\chi d - \xi_M \int d\epsilon\sqrt{\epsilon} f_M(\epsilon)A(\epsilon), \tag{6.7c}$$

$$i\dot{d} = (\tilde{\omega}_0 + \Lambda_d)d - \frac{1}{2}\chi c, \tag{6.7d}$$

$$i\dot{g} = (-\Delta_0 + \Lambda_g)g - \frac{1}{2}\Omega_2 b, \tag{6.7e}$$

$$i\dot{A}(\epsilon) = \epsilon A(\epsilon) - \Omega_1 f_P(\epsilon)b - \alpha f_M(\epsilon)c. \tag{6.7f}$$

Defining $\Lambda_{ij,i\neq j} = \frac{1}{2}\rho\lambda_{ij}$ and $\Lambda_{ij,i=j} = \rho\lambda_{ij}$, $i, j = a, b, c, d, g$, and $\Lambda_{ij} = \Lambda_{ji}$, the shifts in the energy levels due to elastic collisions are

$$\Lambda_i = \sum_j \Lambda_{ij}|x_j|^2. \tag{6.8}$$

Finally, the photodissociation and magnetodissociation couplings are $\xi_P = \Omega/8\pi^2\omega_\rho^{3/2}$ and $\xi_M = \alpha/8\pi^2\omega_\rho^{3/2}$, respectively.

The role of photodissociation has been previously studied [70, 73, 83], and results have found good agreement between the quasicontinuum model and an effective model. Therefore, we simplify the model by treating the dissociated pair amplitude adiabatically ($\dot{A} = 0$), which is equivalent to the limit of weakly bound molecules, and leads to the effective five-level system [Fig. 6.1(b)] with mean-field equations of motion

$$i\dot{a} = \Lambda_a a - \Omega_1 a^* b - \alpha a^* c, \tag{6.9a}$$

$$i\dot{b} = (\tilde{\delta} + \Lambda_b)b - \frac{1}{2}\Omega_1 a^2 - \frac{1}{2}\Omega_2 g - \frac{1}{2}\kappa c, \tag{6.9b}$$

$$i\dot{c} = (\tilde{\nu} + \Lambda_c)c - \frac{1}{2}\alpha a^2 - \frac{1}{2}\chi d - \frac{1}{2}\kappa b, \tag{6.9c}$$

$$i\dot{d} = (\tilde{\omega}_0 - \Lambda_d)d - \frac{1}{2}\chi c, \tag{6.9d}$$

$$i\dot{g} = (-\Delta_0 + \Lambda_g)g - \frac{1}{2}\Omega_2 b. \tag{6.9e}$$

The virtual continuum leads to an effective coupling between the Feshbach and photoassociation molecules of strength

$$\kappa = \frac{1}{8\pi}\frac{\alpha\Omega}{\omega_\rho^{3/2}}\Re\left[\lim_{\epsilon_0\to 0}\int d\epsilon\sqrt{\epsilon}\frac{f_M(\epsilon)f_P(\epsilon)}{\varepsilon - \epsilon_0}\right] \tag{6.10}$$

Additionally, there are real and imaginary shifts for each molecular detuning [73]: $\tilde{\nu} = \nu_0 - \sigma_M - i\gamma_M/2$ and $\tilde{\delta} = \tilde{\delta}_0 - \sigma_P - i\gamma_P/2$, where $\sigma_{M(P)} = \Re[\Sigma_{M(P)}]$ and $\gamma_{M(P)} = \Im[\Sigma_{M(P)}]$ with

$$\Sigma_M = \frac{1}{8}\alpha\xi_M\left[\lim_{\epsilon_0\to 0}\int d\epsilon\sqrt{\epsilon}\frac{f_M^2(\epsilon)}{\varepsilon - \epsilon_0}\right], \tag{6.11a}$$

$$\Sigma_P = \frac{1}{8}\Omega\xi_P\left[\lim_{\epsilon_0\to 0}\int d\epsilon\sqrt{\epsilon}\frac{f_P^2(\epsilon)}{\varepsilon - \epsilon_0}\right]. \tag{6.11b}$$

The real component is the resulting shift of coupling a bound state to a continuum, and the imaginary shift is the dissociation rate, and the shifts are treated as implicit

in the detuning rather than explicitly.

6.2 Results

We focus on parameters based on ^{7}Li homonuclear molecules at low density ($\rho = 10^{12}$ cm^{-3}). The free-bound photoassociation coupling $\Omega_1 = \sqrt{(I/I_0)(\rho/\rho_0)}\Omega_0$, where $\Omega_0 = 290 \times 2\pi$ kHz, $I_0 = 28$ W/cm^2, and $\rho_0 = 4 \times 10^{12}$ cm^{-3}. To set a weak photoassociation coupling, we set an intensity 1/100 of the saturation intensity, $I = 0.28$ W/cm^2. The free-bound magnetoassociation coupling $\alpha_0 = 127 \times 2\pi$ kHz for a typical strong Feshbach resonance. To set a weak magnetoassociation, we set a magnetoassociation coupling 1/100 of the strong coupling, so that $\alpha = (1/100)\alpha_0$. The effective cross-coupling is calculated as $\kappa = 22 \times 2\pi$ kHz. The bound-ground laser coupling is set to $\Omega_2 = 2\Omega_1$, and the bound-bound laser is set to $\chi = 10\Gamma_0$, where Γ_0 is the spontaneous radiative decay $\Gamma_0 = 12 \times 2\pi$ MHz. The spontaneous decay from the photoassociation level is set to $\Gamma_1 = \Gamma_0$ and from the assisting bound-bound level is set to $\Gamma_2 = \Gamma_0$. The losses due to photodissociation is $\gamma_P = I/I_0$ and due to magnetodissociation is $\gamma_M = \alpha^2/8\pi\omega_\rho$. The collision terms are simplified so that $\lambda_{ij,i=j} = \lambda_{ij,i\neq j} = 2\pi\hbar a/\mu$, where the scattering length $a = 100a_0$, and a_0 is the Bohr radius, producing an initial collision strength $\Lambda_0 = 96 \times 2\pi$ Hz, which is stronger than typical collisions for magnetoassociation [145] or photoassociation [74].

To evaluate the system performance, we look at the maximum population of ground state molecules created with the given set of coupling strengths, and varying the detunings to find the optimal parameters, where the population is defined as the wave function probability. By measuring how many ground molecules are created with a certain set of detunings, we are able to determine the optimal detuning values to create a maximum. To determine the relative performance of the laser-assisted system, we compare the maximum ground state molecules created by photoassociation alone ($\alpha = 0, \chi = 0$), and Feshbach-assisted photoassociation only ($\alpha = \alpha, \chi = 0$) at

equal coupling strengths. Finally, we compare how they perform over increases in the collision strength (Λ/Λ_0) by factors of 2, 5, and 10.

The time evolution of the condensate populations is shown in Fig. 6.2. For atoms, $P = |\psi|^2$, while for molecules $P = 2|\psi|^2$. Even with the additional levels explicitly considered in the model, coherent probability oscillates only between atoms and ground state molecules. The photoassociation molecules and assisting laser-bound molecules are effectively dark, while the Feshbach molecules remain dim ($< 1\%$). However, losses due to the Feshbach state are small compared to the photoassociation and laser-bound losses, so in effect, the Feshbach molecules are dark as well. To compare the performance of the systems, only the maximum probability of

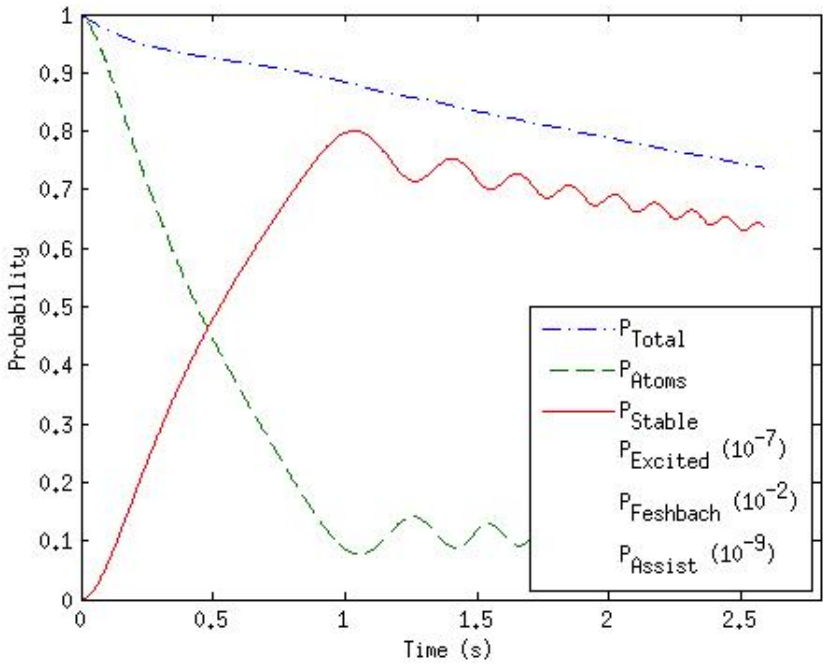

Figure 6.2: Time evolution of probabilities for laser-assisted weak magnetoassociation and weak photoassociation. The dotted-dashed (blue) line is total probability, the dashed (green) line is atomic condensate probability, and the solid (red) line is ground state molecule probability. The probability of excited molecules, Feshbach molecules, and assisting laser-bound molecules remain minute, and are neglected. The magnitude of their max probability is included in the legend.

ground state molecules is considered.

Results comparing the schemes are shown in Fig. 6.3. The results show that both the laser-assisted system and the system with Feshbach enhancement perform better than the system with photoassociation alone. Both create more ground state molecules where collisions are relatively weak, converting about 80% of the initial atomic condensate compared to 55% using photoassociation alone, representing about one and a half times as many molecules. However, when collisions are ten times stronger, the laser-assisted system performs better than both the Feshbach-assisted system and photoassociation alone, still producing about 50% compared to 20% and 15%, respectively.

As expected, magnetoassociation, even with a weak coupling, enhances pho-

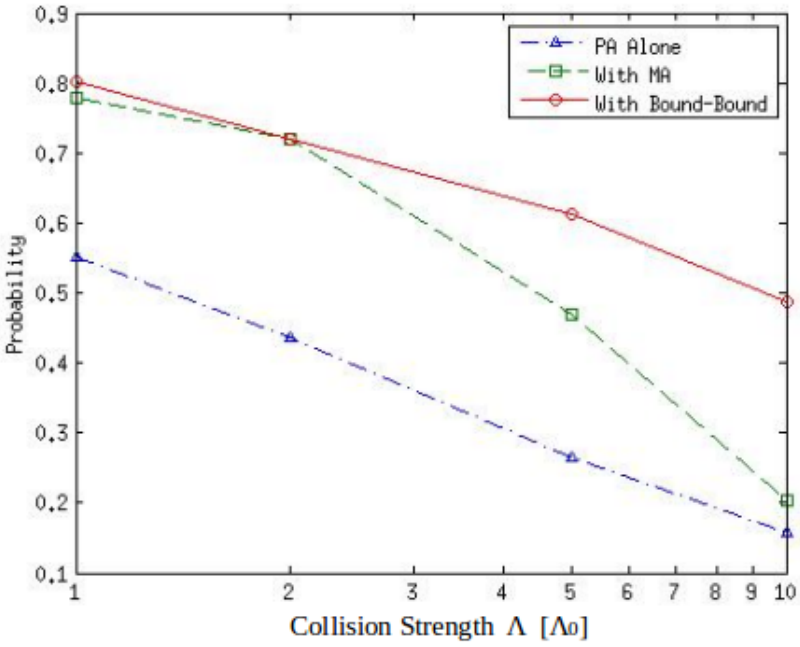

Figure 6.3: Results for laser-assisted Feshbach-enhanced photoassociation. Maximum population of ground state molecules as a function of collisions, relative to initial collision coupling Λ_0. Results for the laser-assisted system (green, dashed) compared to system with photoassociation alone (blue, dashed-dotted) and with Feshbach enhancement only (red, solid).

toassociation, via constructive quantum interference of the bound levels. However, as the collision strengths increase, they reduce the effectiveness of the magnetoassociation enhancement. The improvement stems from the enhancement that magnetoassociation and the assisting laser provide photoassociation over elastic collisions. This is supported by taking an effective resonant-interaction approach to the model [76]. In the case of enhancement from magnetoassociation alone, adiabatically eliminating the Feshbach state ($\dot{c} = 0$) yields the effective coupling strengths

$$\Omega_1' = \Omega_1 - \frac{\alpha\kappa}{2\nu}, \tag{6.12a}$$

$$\Lambda' = \Lambda_{aa} + \frac{\alpha^2}{2\nu}, \tag{6.12b}$$

where Ω_1' is the effective photoassociation coupling strength and Λ' is the effective inter-atomic collision strength. While Raman photoassociation is still explicitly included in the model, magnetoassociation only enters into the system by modifying the photoassociation parameters.

In the case of laser-assisted Feshbach-enhanced photoassociation, in addition to modifying photoassociation, effectively eliminating the Feshbach state also modifies the additional excited bound level coupling strength

$$\alpha' = \frac{\alpha\chi}{2\nu}, \tag{6.13}$$

and the effective cross-molecular coupling

$$\kappa' = \frac{\kappa\chi}{2\nu}. \tag{6.14}$$

To model the effect that the assisting laser has on photoassociation, after adiabatically eliminating the Feshbach state, the assisting state is then adiabatically eliminated ($\dot{d} = 0$). This additionally modifies the photoassociation coupling and

collision strengths

$$\Omega_1'' = \Omega_1' - \frac{\alpha'\kappa'}{2\omega}, \tag{6.15a}$$

$$\Lambda'' = \Lambda' + \frac{\alpha'^2}{2\omega}, \tag{6.15b}$$

The enhancement due to the assisting laser then is dependent on tuning the system parameters so that the effective photoassociation is stronger than the effective collisions.

The effective couplings for each system is shown in Fig. 6.4, using the parameters that produce the results shown in Fig. 6.3, where the effective photoassociation strength is calculated relative to the effective inter-atomic collision strength. As the non-tunable collision strength increases, the photoassociation strength decreases

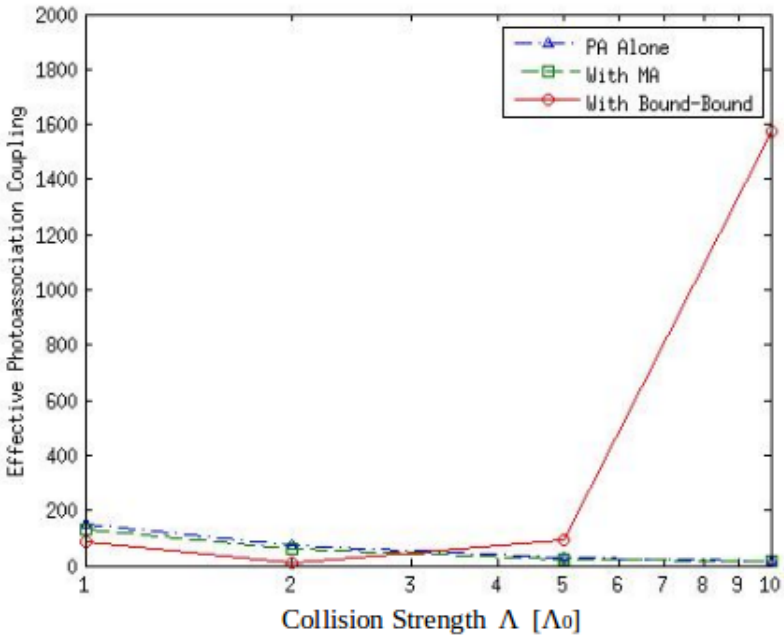

Figure 6.4: Effective photoassociation coupling, relative to the effective collision strength. The dashed-dotted line (blue, triangles) are the bare couplings representing photoassociation alone (Ω_1/Λ), the dashed line (red, circles) represents the effective coupling due to Feshbach enhancement (Ω_1'/Λ'), and the solid line (green, squares) represents the laser-assisted system's effective parameters (Ω_1''/Λ'').

compared to the tunable strength. However, at the strongest non-tunable collision strength, only the laser-assisted system achieves strong enhancement over the tunable collision strength.

The assist from the bound-bound laser then provides the most benefit when overall collisions are at their strongest, while performing comparatively well to the system with magnetoassociation enhancement alone when collisions are weaker. Therefore, the laser-assisting system proves to be more robust over relative increases in collision strengths.

Since the association couplings increase $\propto \sqrt{\rho}$, while collisions increase $\propto \rho$ [74], this also means that the boost the laser-assisted system provides over the other systems should remain as the overall density increases as well. This is seen in Fig. 6.5, where an order of magnitude change in the density does not change the conversion efficiency overall. The improvement due to the assist laser is therefore insensitive to reasonable changes in density.

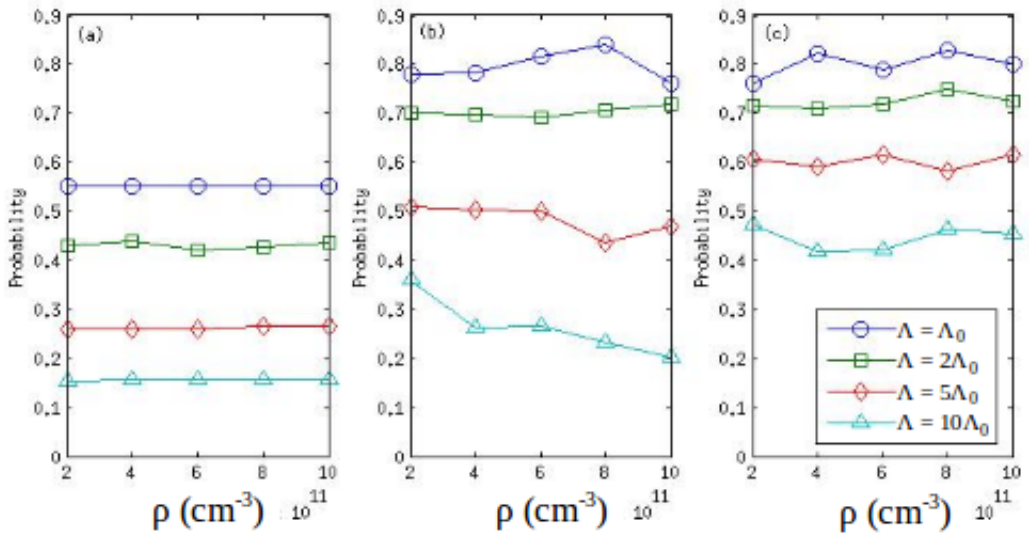

Figure 6.5: Molecule conversion over varying density for (a) photoassociation alone, (b) Feshbach enhancement, and (c) laser-assisted system. Lines represent varying collision strength.

6.3 Summary

We have shown a proof of principle that adding a bound-bound laser to assist weak magnetoassociation and weak photoassociation can improve the efficiency of ground state molecule conversion. The laser-assisted system is generally 30% more efficient than photoassociation alone, and at the strongest collision strength measured, over twice as efficient than either photoassociation alone or Feshbach-enhanced. Compared to the other schemes, the laser-assisted scheme is insensitive to reasonable increases in the density or collision strength, making it more favorable for a wider range of molecular species.

Finally, the laser-assisted system offers more flexibility to optimize the experimental setup based on what is more readily available, whether it is stronger photoassociation lasers, a stronger assisting laser, or a species with wider resonances. There have also been experiments that use frequency-chirped photoassociation to create molecules [146, 147], and utilizing similar techniques could allow for optimizing the detuning over the whole condensate and improve conversion efficiency.

CHAPTER 7

CONCLUSION

Developments in superchemistry and quantum physics have driven interest in cold molecules. They offer a glimpse into the precise interactions and astrophysical constants that constitute our scientific understanding, and a path to future technologies. While much of the research is focused on studying the molecules themselves, creating them in the first place is no trivial matter. With that in mind, we are interested in studying the processes used to create these molecules, and under what conditions would they still reasonably work.

The main objective of this dissertation was to study creating stable quantum degenerate molecules using photoassociation and magnetoassociation. Although these techniques have proven successful under the right conditions, more routine molecules are necessary for many desired applications, such as quantum computing. Furthermore, finding conditions under which photoassociation and magnetoassociation are still effective in a realistic model is vital for adapting these schemes to more complex molecular systems.

In Chapter 2, we began with a simple model that illustrates our methodology. Focusing on photoassociation, we defined the Hamiltonian that we used to derive the equations of motion that described our system. We then developed the numerical algorithms used to solve the system, including a predictor-corrector to account for the nonlinearity. One of the advantages of this system is that further complications can be added without significantly altering the Hamiltonian of the model. As an example, we introduce further complexity by including photodissociation [69].

In Chapter 3, we studied the photoassociation many-body rate limit on atom-molecule conversion [14, 65, 68]. Understanding the rate limit is a vital concept for association and probing the quantum mechanical aspects of these molecules. The rate

limit is set by the time scale at which strong photoassociation depletes the atom-pair wave function, which is determined by the inter-particle spacing. Confirmation was needed on whether the correct time scale coincided with a unitary model or a many body model, especially in the deeply quantum degenerate regime. Consequently, we re-visited the rate limit for atom-molecule conversion with a model that included spontaneous decay [70].

An unanticipated light shift leads to a maximum in the numerical photoassociation loss rate for strong atom-molecule coupling, similarly to the original many-body model without spontaneous decay [68]. With the light shift, the numerical rate saturates at about $9\omega_\rho$, and the many-body rate constant for resonant photoassociation scales with density as $K \propto \rho^{-1/3}$. This limit holds for over two decades of density, where previous analytical results [71, 72] predict this density dependence for limited densities only. The rate limit also agrees with results for combined photoassociation and Feshbach resonance [73], and we found the many-body rate limit to be generally more strict than a two-body unitary rate limit.

In Chapter 4, we investigated stable molecule formation using Raman photoassociation via adiabatic following [74]. Creating stable molecules requires a two-step Raman laser configuration [75], and here we focused on the fixed intensity, varying frequency scenario. This is referred to as adiabatic following, where the ground state of the system "follows" along with an adiabatic change in laser frequency, from atoms to molecules or vice versa, depending on the direction. We looked at two possible schemes, a two-laser configuration and a four-laser configuration. In the two-laser scheme, stable molecules are coupled to the ground state atoms through an electronically excited state, while in the four-laser scheme, transitions to stable molecules occur through an intermediate, vibrationally excited molecular state in the ground electronic manifold.

We found that adiabatic following is a viable means for creating a quantum degenerate gas of stable molecules using practical laser intensities and against strong collisions. The two-laser scheme requires the least photoassociation intensity, about 30 W/cm^2, and is thus more feasible than the four-laser scheme. Collisions cause a DC bias in the frequency, so efficient low-intensity conversion is robust against reasonable increases in the elastic s-wave collision strength. We also expect this scheme to be feasible for heavier species, homonuclear and heteronuclear, based on a study of Li-Na, the lightest (alkali-metal) heteronuclear molecule, and subsequently provides an upper bound on requisite laser intensity [69, 74].

In Chapter 5, we looked at stable molecule formation through Feshbach-enhanced Raman photoassociation [76]. Magnetoassociation, or Feshbach enhancement, offers another method for enhancing photoassociation [66, 77, 78] and bypassing the need for high laser intensity. Focusing on pulsed lasers, we studied both the intuitive scheme, where the pump laser turns on first, and the counterintuitive scheme, where the dump laser turns on first.

Our results confirmed that strong magnetoassociation can substantially improve photoassociation at low intensities, but offers no further improvement at high intensities. The lack of Feshbach enhancement at high intensity is attributed to an already-saturated atom-molecule transition. This improvement is also independent of pulse ordering, which we attribute to an unoptimized pulse length for the counterintuitive pulse order. Disagreement between these models on final conversion efficiencies and the nature of the dark state highlights the importance of explicitly including the Feshbach molecular state in modeling magnetoassociation. Finally, whereas the peak conversion efficiency decreases for stronger intra-atomic, molecular, and atom-molecule collisions, we find that the peak conversion efficiency actually increases for stronger inter-atomic collisions.

In Chapter 6, we investigated whether or not an assisting laser can enhance both weak photoassociation and weak magnetoassociation. In the previous chapter we found that strong magnetoassociation improved molecular conversion of photoassociation at low laser intensity. The question then is whether weak magnetoassociation is capable of enhancing photoassociation in place of strong magnetoassociation if it is backed up by an additional laser. In particular, we couple an assisting laser between the Feshbach state and a bound-bound excited state, which has been shown to enhance magnetoassociation [86, 87], and provides further flexibility regarding the need for strong association.

We found that the assisting laser improved efficiency of ground state molecule formation in the case of weak magnetoassociation and weak photoassociation. The improvement was greatest at the strongest collision strengths tested, and insensitive in reasonable change in condensate density. Finally, the laser-assisted system offers the most flexibility to optimize the experimental setup based on what is more readily available, whether it is stronger photoassociation lasers, a stronger assisting laser, or a species with a wider Feshbach resonance.

7.1 Outlook

In closing, we look at possible subjects for future studies. An interesting direction for this research is to more realistically model experimental conditions by modeling molecular condensates in a trap. This condition introduces an inhomogeneous density, which affects overall association efficiency since association resonance depends on the density. Even though comparisons between thermal and condensate systems should be taken with a grain of salt, the results for Feshbach enhancement in a thermal gas [144] indicate reduced efficiency upon averaging over density, and improved efficiency for narrower Feshbach resonance. Therefore, investigations into condensate inhomogeneity, including an explicit trapping potential, for both wide and

narrow Feshbach resonances will prove highly informative.

Another route for future research is to further investigate the laser-assisted system. The laser-assisted system offers more flexibility over experimental setups, but introduces more parameters to control, making optimization difficult. Developing an adaptive algorithm would therefore improve optimization and reduce computation requirements. Another possible improvement would be to apply pulses to the system and use STIRAP due to its high conversion efficiency. The assist level returns the system into an odd-leveled system, which should establish the dark state on which efficiency is predicated.

Furthermore, applying these methods to create heteronuclear molecular systems offers a rich avenue of future work. For example, heteronuclear alkali-earth molecules give rise to significantly different interactions than bi-alkali dimers [11] and have possible applications in lattice-spin models for quantum computing [148] and measuring the electron permanent electric dipole moment [149]. Molecular ions are another interesting candidate [24], in that they can replace neutral molecules in many of their applications, with the added benefits of being species independent and easily trapped. Finally, Efimov states [21, 22] are of interest for studying three-body recombination [150] and due to their long-lived nature [23], are ideal candidates for studying long-range dipole interactions. Realizing any of these in the quantum degenerate regime would represent a new phase of studies on ultracold molecules.

In conclusion, photoassociation and magnetoassociation offer some of the most promising routes to routine stable quantum degenerate molecules. These methods have already proven to be highly effective, and the focus of this dissertation has only bolstered that assessment. With continued study, photoassociation and magnetoassociation could be the key to considerably easing the requirements to create these molecules in the laboratory, and the multitude of potential applications they repre-

sent. As new milestones in ultracold molecular condensation are achieved, the field of study in these systems is likely to only continue to broaden over time.

BIBLIOGRAPHY

[1] J. M. Hutson, Science **327**, 788 (2010).

[2] R. V. Krems, Physics **3**, 10 (2010).

[3] M. L. Wall and L. D. Carr, Phys. Rev. A **82**, 013611 (2010).

[4] Z. Li and R. V. Krems, Phys. Rev. A **79**, 050701 (2009).

[5] E. A. Cornell and C. E. Wieman, Rev. Mod. Phys. **74**, 875 (2002).

[6] W. Ketterle, Rev. Mod. Phys. **74**, 1131 (2002).

[7] B. Zhu, G. Quéméner, A. M. Rey, and M. J. Holland, Phys. Rev. A **88**, 063405 (2013).

[8] A. M. Jayich, A. C. Vutha, M. T. Hummon, J. V. Porto, and W. C. Campbell, Phys. Rev. A **89**, 023425 (2014).

[9] E. S. Shuman, J. F. Barry, and D. DeMille, Nature **467**, 820 (2010).

[10] S. C. Doret, C. B. Connolly, W. Ketterle, and J. M. Doyle, Phys. Rev. Lett. **103**, 103005 (2009).

[11] J. Ulmanis, J. Deiglmayr, M. Repp, R. Wester, and M. Weidemller, Chemical Reviews **112**, 4890 (2012).

[12] T. Köhler, K. Góral, and P. S. Julienne, Rev. Mod. Phys. **78**, 1311 (2006).

[13] R. Wynar, R. S. Freeland, D. J. Han, C. Ryu, and D. J. Heinzen, Science **287**, 1016 (2000).

[14] C. McKenzie *et al.*, Phys. Rev. Lett. **88**, 120403 (2002).

[15] I. D. Prodan, M. Pichler, M. Junker, R. G. Hulet, and J. L. Bohn, Phys. Rev. Lett. **91**, 080402 (2003).

[16] K. Xu *et al.*, Phys. Rev. Lett. **91**, 210402 (2003).

[17] K.-K. Ni *et al.*, Science **322**, 231 (2008).

[18] B. Pasquiou *et al.*, Phys. Rev. A **88**, 023601 (2013).

[19] H. Hara, Y. Takasu, Y. Yamaoka, J. M. Doyle, and Y. Takahashi, Phys. Rev. Lett. **106**, 205304 (2011).

[20] M. Gacesa, P. Pellegrini, and R. Côté, Phys. Rev. A **78**, 010701 (2008).

[21] V. Efimov, Nuclear Physics A **210**, 157 (1973).

[22] M. D. Lee, T. Köhler, and P. S. Julienne, Phys. Rev. A **76**, 012720 (2007).

[23] Y. Wang, J. P. D'Incao, and C. H. Greene, Phys. Rev. Lett. **106**, 233201 (2011).

[24] E. R. Hudson, Phys. Rev. A **79**, 032716 (2009).

[25] M. Lepers, R. Vexiau, M. Aymar, N. Bouloufa-Maafa, and O. Dulieu, Phys. Rev. A **88**, 032709 (2013).

[26] D. DeMille, Phys. Rev. Lett. **88**, 067901 (2002).

[27] K. Tordrup, A. Negretti, and K. Mølmer, Phys. Rev. Lett. **101**, 040501 (2008).

[28] Y. Huang, Q.-S. Tan, L.-B. Fu, and X. Wang, Phys. Rev. A **88**, 063642 (2013).

[29] M. Yan, B. J. DeSalvo, Y. Huang, P. Naidon, and T. C. Killian, Phys. Rev. Lett. **111**, 150402 (2013).

[30] E. R. Hudson, H. J. Lewandowski, B. C. Sawyer, and J. Ye, Phys. Rev. Lett. **96**, 143004 (2006).

[31] J. Calsamiglia, M. Mackie, and K.-A. Suominen, Phys. Rev. Lett. **87**, 160403 (2001).

[32] Y. P. Huang and M. G. Moore, Phys. Rev. A **73**, 023606 (2006).

[33] O. Dannenberg and M. Mackie, Phys. Rev. A **74**, 053601 (2006).

[34] Q. Dai, F. Zheng, and H. Jing, International Journal of Theoretical Physics **48**, 1348 (2009).

[35] P. D. Nation and M. P. Blencowe, New Journal of Physics **12**, 095013 (2010).

[36] E. Timmermans, P. Tommasini, M. Hussein, and A. Kerman, Physics Reports **315**, 199 (1999).

[37] F. A. van Abeelen and B. J. Verhaar, Phys. Rev. Lett. **83**, 1550 (1999).

[38] V. A. Yurovsky, A. Ben-Reuven, P. S. Julienne, and C. J. Williams, Phys. Rev. A **60**, R765 (1999).

[39] C. A. Regal, C. Ticknor, J. L. Bohn, and D. S. Jin, Nature **424**, 47 (2003).

[40] J. Herbig *et al.*, Science **301**, 1510 (2003).

[41] K. E. Strecker, G. B. Partridge, and R. G. Hulet, Phys. Rev. Lett. **91**, 080406 (2003).

[42] J. Cubizolles, T. Bourdel, S. J. J. M. F. Kokkelmans, G. V. Shlyapnikov, and C. Salomon, Phys. Rev. Lett. **91**, 240401 (2003).

[43] H. R. Thorsheim, J. Weiner, and P. S. Julienne, Phys. Rev. Lett. **58**, 2420 (1987).

[44] R. Napolitano, J. Weiner, C. J. Williams, and P. S. Julienne, Phys. Rev. Lett. **73**, 1352 (1994).

[45] P. D. Lett, P. S. Julienne, and W. D. Phillips, Annual Review of Physical Chemistry **46**, 423 (1995), PMID: 24329894.

[46] K. Burnett, P. S. Julienne, and K.-A. Suominen, Phys. Rev. Lett. **77**, 1416 (1996).

[47] P. S. Julienne, K. Burnett, Y. B. Band, and W. C. Stwalley, Phys. Rev. A **58**, R797 (1998).

[48] J. Javanainen and M. Mackie, Phys. Rev. A **58**, R789 (1998).

[49] P. D. Lett *et al.*, Phys. Rev. Lett. **71**, 2200 (1993).

[50] J. D. Miller, R. A. Cline, and D. J. Heinzen, Phys. Rev. Lett. **71**, 2204 (1993).

[51] E. R. I. Abraham, N. W. M. Ritchie, W. I. McAlexander, and R. G. Hulet, The Journal of Chemical Physics **103** (1995).

[52] H. Wang, P. L. Gould, and W. C. Stwalley, Phys. Rev. A **53**, R1216 (1996).

[53] A. Fioretti *et al.*, Phys. Rev. Lett. **80**, 4402 (1998).

[54] H. Wang and W. C. Stwalley, The Journal of Chemical Physics **108** (1998).

[55] N. Nemitz, F. Baumer, F. Münchow, S. Tassy, and A. Görlitz, Phys. Rev. A **79**, 061403 (2009).

[56] M. Borkowski *et al.*, Phys. Rev. A **84**, 030702 (2011).

[57] D. J. Heinzen, R. Wynar, P. D. Drummond, and K. V. Kheruntsyan, Phys. Rev. Lett. **84**, 5029 (2000).

[58] F. Dalfovo, S. Giorgini, L. P. Pitaevskii, and S. Stringari, Rev. Mod. Phys. **71**, 463 (1999).

[59] B. D. Josephson, Rev. Mod. Phys. **46**, 251 (1974).

[60] P. D. Drummond, K. V. Kheruntsyan, D. J. Heinzen, and R. H. Wynar, Phys. Rev. A **65**, 063619 (2002).

[61] M. Mackie, K. Härkönen, A. Collin, K.-A. Suominen, and J. Javanainen, Phys. Rev. A **70**, 013614 (2004).

[62] F. Lang, K. Winkler, C. Strauss, R. Grimm, and J. H. Denschlag, Phys. Rev. Lett. **101**, 133005 (2008).

[63] J. G. Danzl *et al.*, Nature Physics **6**, 265 (2010).

[64] S. Zhdanovich, E. A. Shapiro, J. W. Hepburn, M. Shapiro, and V. Milner, Phys. Rev. A **80**, 063405 (2009).

[65] M. Junker *et al.*, Phys. Rev. Lett. **101**, 060406 (2008).

[66] P. Pellegrini, M. Gacesa, and R. Côté, Phys. Rev. Lett. **101**, 053201 (2008).

[67] J. Javanainen and M. Y. Ivanov, Phys. Rev. A **60**, 2351 (1999).

[68] J. Javanainen and M. Mackie, Phys. Rev. Lett. **88**, 090403 (2002).

[69] M. Koštrun, M. Mackie, R. Côté, and J. Javanainen, Phys. Rev. A **62**, 063616 (2000).

[70] M. Mackie and P. Phou, Phys. Rev. A **82**, 035602 (2010).

[71] P. Naidon and F. m. c. Masnou-Seeuws, Phys. Rev. A **68**, 033612 (2003).

[72] P. Naidon, E. Tiesinga, and P. S. Julienne, Phys. Rev. Lett. **100**, 093001 (2008).

[73] M. Mackie and C. DeBrosse, Phys. Rev. A **81**, 043625 (2010).

[74] M. Mackie and P. Phou, Phys. Rev. A **82**, 011609 (2010).

[75] M. Gupta and K. R. Dastidar, Phys. Rev. A **81**, 033610 (2010).

[76] M. Mackie, P. Phou, H. Boyce, M. Shinn, and L. Katz, Phys. Rev. A **84**, 043614 (2011).

[77] H. Y. Ling, H. Pu, and B. Seaman, Phys. Rev. Lett. **93**, 250403 (2004).

[78] P.-I. Schneider and A. Saenz, Phys. Rev. A **80**, 061401 (2009).

[79] M. Mackie, M. Fenty, D. Savage, and J. Kesselman, Phys. Rev. Lett. **101**, 040401 (2008).

[80] K. Bergmann, H. Theuer, and B. W. Shore, Rev. Mod. Phys. **70**, 1003 (1998).

[81] I. R. Solá, V. S. Malinovsky, and D. J. Tannor, Phys. Rev. A **60**, 3081 (1999).

[82] Y. Ohta *et al.*, International Journal of Quantum Chemistry **80**, 1068 (2000).

[83] M. Mackie and J. Javanainen, Phys. Rev. A **60**, 3174 (1999).

[84] P. Courteille, R. S. Freeland, D. J. Heinzen, F. A. van Abeelen, and B. J. Verhaar, Phys. Rev. Lett. **81**, 69 (1998).

[85] F. A. van Abeelen, D. J. Heinzen, and B. J. Verhaar, Phys. Rev. A **57**, R4102 (1998).

[86] D. M. Bauer, M. Lettner, C. Vo, G. Rempe, and S. Dürr, Phys. Rev. A **79**, 062713 (2009).

[87] D. M. Bauer, M. Lettner, C. Vo, G. Rempe, and S. Dürr, Nature Physics **5**, 339 (2009).

[88] J. Mostowski and K. Rzazewski, Physics Letters A **66**, 275 (1978).

[89] D. F. Walls and C. T. Tindle, Journal of Physics A: General Physics **5**, 534 (1972).

[90] J. Crank and P. Nicolson, Advances in Computational Mathematics **6**, 207 (1996).

[91] A. F. Linskens, I. Holleman, N. Dam, and J. Reuss, Phys. Rev. A **54**, 4854 (1996).

[92] K. M. Jones, E. Tiesinga, P. D. Lett, and P. S. Julienne, Rev. Mod. Phys. **78**, 483 (2006).

[93] J. Javanainen and M. Mackie, Phys. Rev. A **59**, R3186 (1999).

[94] A. Vardi, V. A. Yurovsky, and J. R. Anglin, Phys. Rev. A **64**, 063611 (2001).

[95] J. J. Hope and M. K. Olsen, Phys. Rev. Lett. **86**, 3220 (2001).

[96] J. L. Bohn and P. S. Julienne, Phys. Rev. A **60**, 414 (1999).

[97] J. Weiner, V. S. Bagnato, S. Zilio, and P. S. Julienne, Rev. Mod. Phys. **71**, 1 (1999).

[98] U. Schlöder, C. Silber, T. Deuschle, and C. Zimmermann, Phys. Rev. A **66**, 061403 (2002).

[99] J. P. Shaffer, W. Chalupczak, and N. P. Bigelow, Phys. Rev. Lett. **82**, 1124 (1999).

[100] A. J. Kerman, J. M. Sage, S. Sainis, T. Bergeman, and D. DeMille, Phys. Rev. Lett. **92**, 033004 (2004).

[101] D. Wang *et al.*, Phys. Rev. Lett. **93**, 243005 (2004).

[102] B. D. Esry, C. H. Greene, J. P. Burke, Jr., and J. L. Bohn, Phys. Rev. Lett. **78**, 3594 (1997).

[103] P. Ao and S. T. Chui, Phys. Rev. A **58**, 4836 (1998).

[104] E. Timmermans, Phys. Rev. Lett. **81**, 5718 (1998).

[105] K. Góral, M. Gajda, and K. Rzążewski, Phys. Rev. Lett. **86**, 1397 (2001).

[106] M. Holland, J. Park, and R. Walser, Phys. Rev. Lett. **86**, 1915 (2001).

[107] A. Görlitz, A. P. Chikkatur, and W. Ketterle, Phys. Rev. A **63**, 041601 (2001).

[108] P. O. Fedichev, Y. Kagan, G. V. Shlyapnikov, and J. T. M. Walraven, Phys. Rev. Lett. **77**, 2913 (1996).

[109] J. L. Bohn and P. S. Julienne, Phys. Rev. A **56**, 1486 (1997).

[110] K. M. Jones, S. Maleki, L. P. Ratliff, and P. D. Lett, Journal of Physics B: Atomic, Molecular and Optical Physics **30**, 289 (1997).

[111] J. M. Gerton, B. J. Frew, and R. G. Hulet, Phys. Rev. A **64**, 053410 (2001).

[112] C. Pethick and H. Smith, *Bose-Einstein Condensation in Dilute Gases* (Cambridge University Press, 2002).

[113] Y. B. Band and P. S. Julienne, Phys. Rev. A **51**, R4317 (1995).

[114] J. L. Bohn and P. S. Julienne, Phys. Rev. A **54**, R4637 (1996).

[115] R. Dum, J. I. Cirac, M. Lewenstein, and P. Zoller, Phys. Rev. Lett. **80**, 2972 (1998).

[116] A. Ishkhanyan, M. Mackie, A. Carmichael, P. L. Gould, and J. Javanainen, Phys. Rev. A **69**, 043612 (2004).

[117] M. H. Anderson, J. R. Ensher, M. R. Matthews, C. E. Wieman, and E. A. Cornell, Science **269**, 198 (1995).

[118] C. C. Bradley, C. A. Sackett, J. J. Tollett, and R. G. Hulet, Phys. Rev. Lett. **75**, 1687 (1995).

[119] K. B. Davis *et al.*, Phys. Rev. Lett. **75**, 3969 (1995).

[120] J. Kobayashi, K. Aikawa, K. Oasa, and S. Inouye, Phys. Rev. A **89**, 021401 (2014).

[121] P. Ehrenfest, Annalen der Physik **356**, 327 (1916).

[122] M. Born and V. Fock, Zeitschrift fr Physik **51**, 165 (1928).

[123] T. Kato, Journal of the Physical Society of Japan **5**, 435 (1950).

[124] D. M. Tong, Phys. Rev. Lett. **104**, 120401 (2010).

[125] M. H. S. Amin, Phys. Rev. Lett. **102**, 220401 (2009).

[126] N. Balakrishnan, R. C. Forrey, and A. Dalgarno, Phys. Rev. Lett. **80**, 3224 (1998).

[127] K. Winkler *et al.*, Phys. Rev. Lett. **95**, 063202 (2005).

[128] V. Vuletić, C. Chin, A. J. Kerman, and S. Chu, Phys. Rev. Lett. **83**, 943 (1999).

[129] B. L. Tolra *et al.*, EPL (Europhysics Letters) **64**, 171 (2003).

[130] U. Gaubatz, P. Rudecki, S. Schiemann, and K. Bergmann, The Journal of Chemical Physics **92** (1990).

[131] M. Mackie, R. Kowalski, and J. Javanainen, Phys. Rev. Lett. **84**, 3803 (2000).

[132] J. Oreg, K. Bergmann, B. W. Shore, and S. Rosenwaks, Phys. Rev. A **45**, 4888 (1992).

[133] G. W. Coulston and K. Bergmann, The Journal of Chemical Physics **96** (1992).

[134] V. S. Malinovsky and D. J. Tannor, Phys. Rev. A **56**, 4929 (1997).

[135] N. V. Vitanov and S. Stenholm, Phys. Rev. A **60**, 3820 (1999).

[136] B. Deb and G. S. Agarwal, Journal of Physics B: Atomic, Molecular and Optical Physics **42**, 215203 (2009).

[137] S. Kotochigova, T. Zelevinsky, and J. Ye, Phys. Rev. A **79**, 012504 (2009).

[138] D. Skouteris *et al.*, Science **286**, 1713 (1999).

[139] E. Garand, J. Zhou, D. E. Manolopoulos, M. H. Alexander, and D. M. Neumark, Science **319**, 72 (2008).

[140] E. Charron, P. Milman, A. Keller, and O. Atabek, Phys. Rev. A **75**, 033414 (2007).

[141] T. Köhler, E. Tiesinga, and P. S. Julienne, Phys. Rev. Lett. **94**, 020402 (2005).

[142] W. C. Stwalley, Phys. Rev. Lett. **37**, 1628 (1976).

[143] E. Tiesinga, B. J. Verhaar, and H. T. C. Stoof, Phys. Rev. A **47**, 4114 (1993).

[144] A. C. Han, E. A. Shapiro, and M. Shapiro, Journal of Physics B: Atomic, Molecular and Optical Physics **44**, 154018 (2011).

[145] M. Mackie, Phys. Rev. A **66**, 043613 (2002).

[146] E. Luc-Koenig, R. Kosloff, F. Masnou-Seeuws, and M. Vatasescu, Phys. Rev. A **70**, 033414 (2004).

[147] C. P. Koch, E. Luc-Koenig, and F. m. c. Masnou-Seeuws, Phys. Rev. A **73**, 033408 (2006).

[148] A. Micheli, G. K. Brennen, and P. Zoller, Nature Physics **2**, 341 (2006).

[149] E. R. Meyer and J. L. Bohn, Phys. Rev. A **80**, 042508 (2009).

[150] A. Härter *et al.*, ArXiv e-prints **1301.5518** (2013).